Effects of mixed solvents on the structural morphology and membrane distillation performance of PVDF-HFP hollow fiber membranes

L. García-Fernández [1], M.C. García-Payo [1], M. Khayet [1,2,*]

[1] Department of Applied Physics I, Faculty of Physics, University Complutense of Madrid, Av. Complutense s/n, 28040, Madrid, Spain.

[2] Madrid Institute for Advanced Studies of Water (IMDEA Water Institute), Calle Punto Net Nº 4, 28805, Alcalá de Henares, Madrid (Spain).

* Corresponding author: khayetm@fis.ucm.es

Tel. +34-91-3945185

Fax. +34-91-3945191

Abstract

Poly(vinylidene fluoride-hexafluoropropylene), PVDF-HFP, hollow fiber membranes were prepared by the dry/wet spinning technique, maintaining all the parameters the same except the solvent used to prepare the polymer solution. Different solvents namely, single *N*,*N*-dimethyl acetamide (DMAC) and different mixed solvents (DMAC and trimethyl phosphate (TMP) as well as *N*,*N*-dimethyl formamide (DMF) and TMP were employed. The relative affinity of the PVDF-HFP and the solvent(s) and the thermodynamic and kinetic aspects responsible for membrane formation were investigated and related with the structure of the prepared hollow fiber membranes. The structural and morphological properties of the hollow fiber membranes as well as the necessary parameters to be known for a membrane proposed for direct contact membrane distillation (DCMD) were studied by different characterization techniques. It was observed that an increase of TMP ratio in the solvents mixture resulted in a decrease of the finger-like structure of the external layer, an increase of the pore sizes of the hollow fibers and the DCMD permeate flux enhancement as consequence. When changing DMAC by DMF a thicker hollow fiber membrane was obtained and the DCMD was decreased due partly to the formation of macro-voids in the middle layer of the hollow fiber membrane.

Keywords:

Hollow fiber membrane; Membrane Distillation; Poly(vinylidene fluoride-hexafluoropropylene); Desalination; Solvent effect.

1. Introduction

Membrane distillation (MD) is a non-isothermal separation process in which only molecules in vapour phase are transported through a porous and hydrophobic membrane. Recently, MD has received an increasing and special attention (design and fabrication of novel membranes and modules, coupling MD installations to renewable energy systems, development of theoretical models and optimization of MD plants, etc.) [1,2]. The permeability, wetting resistance, long-term stability, energy efficiency and solute rejection or separation factors of MD process are dependent on membrane properties [1-3]. Moreover, the membrane pore structure and morphology play a significant role on the mass and heat transport properties in MD as well as on the mechanical strength of the membrane. During last seven years, membrane fabrication and its performance improvement received a progressive attention by various worldwide research groups, with special interest in hollow fiber membranes due to their high membrane surface area per unit volume resulting in a high permeate production rate, good flexibility in operation, mechanically self-supporting and are easily assembled into modules [1,2,4-11].

Most hollow fiber membranes are prepared by the dry/wet spinning technique although it is a complex process that involves many operating parameters (dope composition, pressure applied on the dope solution, temperature, air gap distance between the spinneret and the external coagulant, nature of the internal and external coagulants, flow rate of the internal coagulant, structure and dimensions of the spinneret, fiber take-up speed, etc.) [12-18]. The morphology, mechanical properties and the performance of hollow fibers are affected by various spinning conditions. The interaction effects between the spinning parameters also play an important role to obtain an optimum hollow fiber membrane [12,19,20]. Therefore, it is not an easy task to

identify the adequate spinning conditions for a given polymer. Moreover, up to date understanding the mechanisms of hollow fiber membrane formation is rather qualitative than quantitative.

Recently, the copolymer poly(vinylidene fluoride-*co*-hexafluoropropylene) (PVDF-HFP) has received much attention as a highly promising material for membrane fabrication for various membrane processes [21-28]. Fluorine content of PVDF-HFP is higher than that of poly(vinylidene fluoride) (PVDF) due to hexafluoropropylene (HFP) group, which makes PVDF-HFP more hydrophobic than PVDF. As a consequence, PVDF-HFP is a potential candidate in applications requiring membranes with higher hydrophobicity such as MD technology.

The reduction of the copolymer concentration in the spinning solution is one of the explored options to improve the membrane permeability but mechanical strength might be sacrificed [20,24,28]. Additives or pore formers are often used. Shi et al. [22,23] used polyvinylpyrrolidone (PVP), lithium chloride (LiCl) and glycerol as additives for fabrication of PVDF-HFP hollow fibers. It was found that the prepared fibers presented different structures with different additives. LiCl or glycerol addition made the resultant membranes exhibit a narrower pore size distribution than that fabricated with the additive PVP. The hydrophobic property of the membranes was affected by three additives in the sequence of PVP > LiCl > glycerol. Moreover, the use of mixed additives, LiCl with Tween 80, and PVP with glycerol, resulted in the development of finger-like macro-voids [27]. Feng et al. [24] reported on the preparation of PVDF-HFP flat sheet asymmetric membranes for direct contact membrane distillation (DCMD) and studied the effects on pore structure and permeate performance of different factors such as polyethylene glycol (PEG) molecular weight, type of additive (i.e. PEG or glycerol), temperature of the external coagulant and its type. Cao et al. [29] used dibutyl phthalate

(DBP), PEG and PVP as additives for preparation of PVDF-HFP membranes. The membranes prepared with DBP and PEG exhibited an asymmetric structure and relatively small pore sizes; whereas nearly symmetric and microporous structures were observed when PVP was used as additive. PEG was also used by Hwang et al. [30] and found that the morphology of the PVDF-HFP membranes changed considerably with the composition of the polymer and solvent. Recently, Wongchitphimon et al. [31] revealed that the addition of PEG in PVDF-HFP/ *N*-methyl-2-pyrrolidone (NMP) solution resulted in a system thermodynamically less stable in reaction with water, promoting rapid phase demixing in the phase inversion process. When 3 wt.% PEG was added in the polymer solution, it was observed an increase in the dimension of finger-like macro-voids of the membrane with the increase of PEG molecular weight from 200 to 600 and 6000 kDa, enhancing therefore the membrane water permeability .

It is clear that the kinetic parameters of a polymer solution such as the exchange rate between solvent and nonsolvent as well as the thermodynamic parameters such as the polymer-solvent interaction, solvent–nonsolvent interaction are necessary to understand in order to explain and predict a membrane structure [13,32]. For instance, the selection of the solvent necessary to prepare the polymer solution plays a key role in membrane fabrication. The thermodynamic interaction between the polymer and solvent (i.e. the compatibility between the polymer and solvent) does not only affect the ternary phase diagram (solvent-polymer-nonsolvent) but also the kinetics pore growth [33,34]. As a result, the morphology and performance of the membrane may be predicted and controlled by selecting the appropriate solvent(s). Besides, by evaporating the solvent from the outer surface of the as-spun hollow fiber through the dry phase, air gap between the spinneret and the external coagulation bath, the cross section structure of the membrane can be modified.

Although it is well known that polymer coagulation is due to solvent exchange with nonsolvent affecting considerably the formed membrane structure, with the exception of few early studies, experimental measurements of the solvent-nonsolvent exchange rate and the additive leaching rate during polymer coagulation are very scarce. Recently, some studies appeared on the kinetics of polymer coagulation, but they are mainly focused on ternary systems formed by PVDF, a single solvent and a nonsolvent [33-36]. However, no study is found on the effects of mixed solvents on PVDF or PVDF-HFP hollow fiber membrane structure.

Yeow et al. [37] compared the morphology of flat sheet PVDF membranes prepared with different solvents, NMP, *N*,*N*-dimethyl formamide (DMF), *N*,*N*-dimethyl acetamide (DMAC) and triethyl phosphate (TEP). The scanning electron microscopy (SEM) images of these membranes showed a symmetrical sponge-like structure through the whole membrane thickness without cavities when using TEP (i.e. the poorest solvent), but the membrane prepared with the solvent NMP exhibited irregular macro-voids beneath the top skin layer. In the case of the solvents DMF and the strongest solvent DMAC, the PVDF membrane cross-sectional structure exhibited similar short finger-like structure with sponge substrates indicating a slow exchange rate between the solvent and nonsolvent.

Ong et al. [38], by preparing flat sheet asymmetric PVDF membranes with the solvents mixtures (NMP/tetrahydrofuran (THF) or NMP/acetone) and evaporation of the solvents THF and acetone, observed other than the formation of a dense skin top layer the suppression of macro-voids from the cross-section of the membrane. Li et al. [39] also used mixed solvents to prepare PVDF flat sheet membranes and found that the membrane prepared with 60 wt.% of trimethyl phosphate (TMP) and 40 wt.% of DMAC exhibited the highest permeate flux but a low salt rejection factor. Recently, Li

et al. [40] used a dual coagulation process to further improve the PVDF membrane hydrophobicity and prevent the formation of the dense skin layer of flat sheet membranes. The solution casting film was first immersed for 30 s in a mixture of water and the (TEP–DMAC) solution (i.e. the first coagulation bath) followed by immersion in water (i.e. the second coagulation bath). An increase of the TEP–DMAC content in water changed the morphological structure of the membrane from an asymmetric structure with a dense top layer to a symmetric structure with a skinless top layer, while the pore size distribution turned to be narrower. Moreover, by increasing the mass ratio of TEP to DMAC in the polymer solution, the dense top layer of the membrane surface decreased significantly.

The purpose of this study is to investigate the effects of the solvent type on the PVDF-HFP hollow fiber membrane structure, membrane parameters and DCMD performance. Single (DMAC) and mixed solvents (DMAC/TMP and DMF/TMP) have been considered. Attempts are made to correlate the solvent(s) used to prepare the spinning solutions to the characteristics and final DCMD performance of PVDF-HFP hollow fiber membranes.

2. Experimental

2.1 Materials

The spinning solutions were prepared from the copolymer poly(vinylidene fluoride-co-hexafluoropropylene) (PVDF-HFP; M_w = 455,000 g/mol), the solvents *N*,*N*-dimethyl formamide (DMF), *N*,*N*-dimethyl acetamide (DMAC) and trimethyl phosphate (TMP) and the nonsolvent additive poly(ethylene glycol) (PEG; M_w = 6000 g/mol). Isopropyl alcohol (IPA) was used as a wetting liquid for the measurements of the void volume fraction and sodium chloride (NaCl) to prepare the salt aqueous feed

solutions for DMCD experiments. All these chemicals were purchased from Sigma-Aldrich Chemical Co, except NaCl that was purchased from Panreac.

2.2 Preparation and characterization of the spinning solutions

5 wt.% of the nonsolvent additive (PEG) was first dissolved in 76 wt.% of the solvent(s) at 42ºC and 100 rpm using a magnetic stirrer (IKA, RCT basic). Based on the conclusions drawn by Li et al. [39], the used solvent was DMAC, its mixture with TMP at different ratios (40 and 60 wt.%) and the mixture TMP/DMF (40 wt.%) as indicated in Table 1. After getting an homogenous mixture, 19 wt.% of PVDF-HFP was added to this mixture and the whole solution was introduced in a thermal bath (Stuart SBS40) maintained at 42ºC under an orbital shaker until the whole copolymer was totally dissolved.

2.2.1 Thermodynamic experiment: cloud point

It is convenient to study the ternary phase diagram in order to understand the thermodynamic behavior of a given phase inversion membrane formation process. Thermodynamic analysis reveals the effects of interaction of blend components during their mixing/demixing steps. The ternary phase diagram was plotted for the used system copolymer/single or mixed solvents/nonsolvent. The cloud point of this system was determined for each spinning solution by turbidimetric titration method at the same temperature used for preparation of hollow fiber membranes (42ºC). It is known that the cloud point depends on the temperature [36]. The nonsolvent water, 20 μl, was added stepwise in the PVDF-HFP spinning solution by means of a burette and a gentle stirring using a magnetic stirrer (IKA, RCT basic) at 250 rpm. The necessary quantity of water turning the spinning solution turbid is assigned as the cloud point.

2.2.2 Kinetic experiments: solvent evaporation and PVDF-HFP coagulation

Asymmetric hollow fiber membranes exhibiting a thin and relatively dense skin layer and a more open porous substrate are commonly produced by the dry/wet spinning technique. The skin layer is mainly due to the partial solvent evaporation involved in the dry phase inversion step through the air gap between the spinneret and the external coagulation bath. Therefore, kinetic studies on the rate of solvent evaporation in the dry step and the solvent-nonsolvent exchange rate in the wet step are essential to understand and subsequently control the membrane structure.

Solvent evaporation study was carried out by casting a flat sheet PVDF-HFP film on a glass plate at 42ºC and recording the weight change with time of the cast film together with the glass plate. In this test, the same PVDF-HFP solutions prepared for fabrication of hollow fiber membranes were used. All the flat sheet films were fabricated following the same procedure under the same operating conditions.

The solvent-nonsolvent exchange rate of the PVDF-HFP solutions was studied by light transmittance test. The set-up consists of a low-pressure sodium (LPS) employed as light source. The casting PVDF-HPF solution was immersed in a water coagulation bath and the evolution of the transmitted light was detected by a photodiode at wavelength of 589 nm. The coagulation rate of the PVDF-HFP in the coagulation bath was determined by the obtained normalized light transmittance curve over time. The normalized light transmittance was calculated as follows [41]:

$$T_{norm} = \frac{T - T_{min}}{T_{max} - T_{min}}, \quad (1)$$

where T_{norm} is the normalized light transmittance, T_{min} is the minimum transmittance and T_{max} is the maximum transmittance.

2.2.3 Viscosity and surface tension of the spinning solutions

The viscosity of the spinning solution was measured by a Digital Viscometer (Brookfield, Model DV-I+) using a cylindrical sample container, which permits to keep constant the temperature of the spinning solution by a thermostat (Techne, Model TU-16D). In this study, the viscosity was measured at 42 ºC with the LV1 spindle at 1 rpm and a shear rate of 0.22 s^{-1}.

The surface tension of the spinning solution was determined at room temperature by the pendant drop shape analysis using an optical contact angle meter (CAM 200) and a stainless steel needle having an outer diameter of 1.832 mm. The drop volume of all samples was kept constant at 12.4 µL.

2.3 Preparation of hollow fiber membranes and their characterization

The dry/wet spinning technique was employed to prepare the hollow fiber membranes as described elsewhere [28]. Table 2 summarizes the spinning parameters, which were maintained the same except the solvent used to prepare the spinning solutions. After spinning, the fabricated hollow fiber membranes were stored in water bath at room temperature for 48 h to remove the residual solvent. Subsequently, the hollow fiber membranes were dried at room temperature before characterization tests.

The inner and outer diameters of the prepared PVDF-HFP hollow fiber membranes were measured by means of an optical microscope (OLYMPUS BX60M) with a precision of ± 1 µm. The internal structure of the membranes was studied by the field emission scanning electron microscope (FESEM, JEOL Model JSM-6335F). The

samples were first fractured in liquid nitrogen and then sputter-coated with a thin layer (5 nm) of gold using an evaporator (EMITECH K550 X) for one minute under 25 mA.

The void volume fraction (i.e. porosity, ε) was determined following the method described in previous studies [28,42].

The roughness, the mean pore size and the pore size distribution of both the internal and external surfaces of the PVDF-HFP hollow fibers were studied by atomic force microscopy (AFM). The AFM images were obtained using a tapping mode Nanoscope III equipped with 1553D scanner (Digital Instruments Inc., Santa Barbara, Ca). The same tip was used to scan the surfaces of all samples and all captured images were treated in the same way as described elsewhere [15,16]. The followed methods to evaluate the mean roughness and the mean pore size and determine the pore size distribution were explained in details in [16,42].

The liquid entry pressure (*LEP*) in the membrane pores is the highest applied transmembrane pressure on a liquid solution before this penetrates into the pores [28,43]. This is an important parameter to be known for a given membrane before its use in any MD application. In fact, *LEP* must be as high as possible. In this study, a salt aqueous solution (NaCl, 3 wt.%) was used to determinate the *LEP* using the experimental set-up schematized in Fig. 1. Four hollow fibers having a length of about 8 cm were assembled in a stainless steel tube with an epoxy resin. One side of the fibers was closed while the other side was connected to the outlet of a pressurized tank (SARTORIUS, SM 16249). The module was submerged in a container filled with distilled water as shown in Fig. 1. After the pressurized tank was filled with the salt aqueous solution, a slight pressure was applied on the hollow fiber membrane for at least 20 min. Subsequently, the applied pressure was increased stepwise by means of a

pressure valve. In order to register a correct electrical conductivity by a conductivity meter (EUTECH Instruments, ECCON1103K), distilled water was stirred using a magnetic stirrer (EYELA RC-2). When the salt solution enters the membrane pores, a change in the electrical conductivity of water in the container is detected. These measurements were performed using three different samples for each PVDF-HFP hollow fiber membrane.

A gas-liquid displacement Porometer (POROLUX™ 100, Porometer) was also used to determine pore size of the hollow fiber membranes. First, a wet curve was obtained by measuring the air flow rate as a function of the difference applied transmembrane pressure using a sample previously submerged in a wetting liquid (POREFIL®, Porometer). Subsequently, a dry curve was obtained following the same procedure. The mean pore size was then determined using both wet and dry curves with the computer software (POROLUX100, Porometer) as described elsewhere [44]. Additionally, the mean pore size and the effective porosity (ε/L_p) were evaluated from the dry curve only following the gas permeation method described elsewhere [42]. ε/L_p is defined as the ratio of the porosity and the effective pore length that takes into account the tortuosity of the membrane pores.

Differential Scanning Calorimetry (DSC) tests were performed with a Mettler-Toledo DSC 1, STAR^e System. The measurements were carried out in a nitrogen atmosphere at flow rate of 20 ml/min. Samples from 3.21 to 4.35 mg were placed in standard aluminum pans of 100 µl capacity. The samples were heated at a rate of 15^{o}C/min from 35^{o}C to 200^{o}C and then cooled down at the same speed. The melting (T_m) and the crystallization (T_c) temperatures correspond to the minimum and maximum peaks of the obtained curves, respectively; while the enthalpy of melting (ΔH_m) and

enthalpy of crystallization (ΔH_m) were obtained from the area of the endothermic and exothermic peaks, respectively. The degree of the crystallinity of the samples was estimated as follows:

$$\chi_c(\%) = \frac{\Delta H_m}{{\Delta H_m}^o} \times 100 \quad (2)$$

where ${\Delta H_m}^o$ is the standard fusion enthalpy for a 100% crystalline polymer, which is 104.7 J/g for PVDF-HFP [45,46].

2.4 Direct contact membrane distillation experiments

DCMD experiments were carried out using the experimental set-up shown in Fig. 2. Tubular PVDF-HFP hollow fiber membrane modules were first prepared. Six hollow fiber membranes were cut and packed in a stainless-steel shell-and-tube module using epoxy resin at both ends. The effective length of the hollow fiber membranes is 20 cm. The feed and permeate circulated tangentially to the membrane in a counter-current way. The feed solution was circulated through the lumen side of the membrane module, while the permeate (distilled water) was circulated through its shell side. Both the feed and permeate circulated through the membrane module by means of a double-head peristaltic pump (5) (Watson Marlow 323). First, DCMD experiment was carried out using distilled water as feed to check if there is any loss of water in the set-up. Subsequently, DCMD experiments were carried out using a salt aqueous solution (NaCl, 3 wt.%) as feed. The permeate flow rate was determined from the registered mass of produced water over time using a precision balance (10) (Gibertini Europe 3000) connected to a computer (11). The permeate flux was calculated based on the inner fiber surface area. The feed and permeate temperatures were controlled by means of a heating (3) (Techne, model TE-8D) and a cooling (4) (Polysciences, model 6206T) thermostats, respectively. The feed and permeate containers were connected to the

corresponding thermostats by glass heat exchangers. Pt-100 probes (7) were installed at both the inlets and outlets of the membrane modules and were connected to the computer (11) using own software developed by our research group that recorded the values of both the mass of produced water and temperatures automatically every 30 s. The feed inlet temperature was varied from 50 to 80ºC while the permeate inlet temperature was kept at 25ºC. The feed flow rate (circulated through the lumen side of the membrane module) was kept at 13.8 ± 1.2 kg/h, whereas the permeate circulated through the shell side was kept at 20.7 ± 0.6 kg/h. The membrane module and all tubes were insulated. At the beginning and the end of each DCMD experiment, samples of both the feed and permeate were extracted to measure their electrical conductivity by a conductivity meter (Metrohm model 712) and then determine the salt concentration and the salt rejection factor.

3. Results and discussions

3.1 Spinning solution characterization

3.1.1 PVDF-HFP/mixed solvent/PEG interactions

The relative affinity of PVDF-HFP and the solvent or the mixtures of solvents can be assessed using the Hansen's solubility parameter, *HSP*, (δ_t), which includes a polar component (δ_p), a dispersion force component (δ_d), and a hydrogen bonding component (δ_h) [47]. Since materials with similar values of δ_t are likely to be miscible, the interaction between PVDF-HFP and the solvent can be defined as *HSP* distance (R_{HSP}) following the equation [47]:

$$R_{HSP} = \left[4(\delta_{ds} - \delta_{dc})^2 + \left(\delta_{ps} - \delta_{pc}\right)^2 + (\delta_{hs} - \delta_{hc})^2\right]^{1/2} \quad (3)$$

where the subscripts *s* and *c* refer to the single solvent or the mixture of solvents and the copolymer PVDF-HFP, respectively. The lower is the distance R_{HSP}, the better is the solvent. *HSP* of solvents mixture can be calculated with the volume fraction weighted average of *HSP* components [48]:

$$[\delta_{dm}, \delta_{pm}, \delta_{hm}] = [a\delta_{d1} + b\delta_{d2}, a\delta_{p1} + b\delta_{p2}, a\delta_{h1} + b\delta_{h2}]/(a + b) \quad (4)$$

where the subscripts 1 and 2 are for each single solvent present in the mixture, *m* is the solvents mixture, and *a* and *b* are the volume fraction of the different solvents in the mixture. Table 3 lists the solubility parameters of PVDF-HFP [49], PEG [31], DMAC, DMF and TMP [47]. It can be seen that the value of R_{HSP} for the pair *P-S* (PVDF-HFP and DMAC or mixtures of DMAC and TMP) is smaller than those of DMF and TMP indicating that the affinity of PVDF-HFP with DMAC is better than that with the other studied solvents. In conclusion, DMAC demonstrated to be the strongest solvent to PVDF-HFP. The value of R_{HSP} for the pair (*P-S*) increased with the increase of the TMP amount in the solvent mixture. This means a less interaction of the PVDF-HFP copolymer chains with the solvents mixture making easier the diffusion of the solvent from the spinning solution. As summarized in Table 3, no significant change was detected in the R_{HSP} values for water-solvent (*W-S*) interaction for the spinning solutions DMAC100, DMAC60 and DMAC40. However, when DMAC was changed by DMF in the solvent mixture, R_{HSP} (*P-S*) was enhanced whereas R_{HSP} (*W-S*) was reduced improving further the affinity between water and the solvents and making easier the interdiffusion between water and the solvent(s) during coagulation process.

The viscosity of the spinning solution is also an important parameter exerting a strong influence on the interdiffusion of solvent and nonsolvent during the coagulation process and therefore affecting the kinetics of the phase inversion during membrane

formation. It is believed that an enhancement of the viscosity reduced the coagulation rate of the polymer solution [39]. Table 1 presents the obtained viscosity of the studied spinning solutions. The order of magnitude of these values is the same as that of PVDF-HFP at 23 ^{o}C [31] and PVDF [35] solutions measured at 25 ºC. As the amount of TMP was increased in the solvents mixture a significant enhancement of the viscosity was observed resulting in a high resistance to water/solvent interdiffusion during PVDF-HFP membrane formation. Moreover, a reduction of the viscosity of the spinning solution was observed when changing DMAC with DMF favoring the water/solvent exchange during PVDF-HFP coagulation.

As it is summarized in Table 1, the surface tension of the spinning solution decreased with increasing the amount of TMP in the DMAC mixture and it is higher for DMF60 than for DMAC60. These results are attributed partly to the higher surface tension of the corresponding used solvent(s) (e.g. the surface tension of DMF is higher than that of DMAC). Decreasing the surface tension of the polymer solution reduced the die-swell effect at the exit of the spinneret. Moreover, it was verified that increasing the polymer solution viscosity also minimized the die-swell effect [50]; and high die swell resulted in greater outer and inner fiber diameters [51]. This statement is applicable for the hollow fiber membranes DMAC60 and DMAC40, when the concentration of TMP was increased; and for DMF60 and DMAC60, when the solvent DMF was changed to DMAC. In both cases (i.e. increase of the TMP concentration from 40 to 60 wt.% and use of DMAC instead of DMF) the viscosity was increased whereas the surface tension was decreased as can be seen in Table 1. Both led to a decrease of the die-swell effect and both the inner and outer fiber diameters were reduced considerably (Table 5). For the hollow fiber membranes DMAC100 and DMAC60, no clear relationship can be obtained if the standard errors of the diameters are considered.

The surface tension effect may be related with the die-swell and fiber diameters as a consequence, but this effect can be counterbalanced by the elongational stress along the air gap distance due to gravitational force. In this study, as it will be explained later on, it was found greater fiber diameters and thickness of the membrane DMF60 prepared with higher surface tension spinning solution than the membrane DMAC60 (Table 5).

3.1.2 Thermodynamic and kinetics experiments

Figure 3 shows the developed ternary phase diagram representing phase separation of the studied spinning solutions prepared with different solvents. The stronger is the solvent power, the greater is the amount of nonsolvent (water in this study) required to induce PVDF-HFP precipitation. When the amount of TMP in the solvent mixture was increased, the cloud point shifted away from the PVDF-HFP / PEG – water axis towards the PVDF-HFP / PEG - solvent axis. This effect was more pronounced when DMF was used instead DMAC. The amount of water required for PVDF-HFP coagulation (i.e. cloud point) decreased following the order (the thermodynamically less stable spinning solution): DMF60 < DMAC40 < DMAC60 < DMAC100. This result agrees with the reported values of R_{HSP} for the pair (*P*-*S*) in Table 3. The thermodynamic results indicate that the increase of the TMP rate in the spinning solution and the use of the solvent DMF instead of DMAC both cause an earlier phase separation. It is known that the morphological structure of a membrane precipitated by liquid/liquid demixing depends on the position of the polymer solution in the ternary phase diagram and for the polymer concentration above the critical point demixing occurs by nucleation of the polymer lean phase resulting in a porous structure, which will be more or less open depending on the time available for droplets coalescence. However, when the polymer concentration is low, demixing takes place by nucleation of the polymer-rich phase giving rise to a latex-type structure. The structure of the hollow fiber membranes

prepared in this study with different types of solvents will be explained based on the obtained SEM images taking into consideration this phenomenon.

The kinetics of solvent evaporation can be described quantitatively. Sun et al. [34] reported that the temperature and film-casting thickness affected the solvent evaporation rate significantly. In this study both parameters were maintained constant and only the effect of the mixed solvents was investigated. The partial evaporation of the solvent from the surface of the nascent membrane in the dry step (along the air gap in the case of hollow fiber spinning) affects not only the outer skin layer of the as-spun fiber but also the polymer coagulation from the inner wet side of the fiber. Figure 4 shows the relative quantity of the evaporated solvent ($(W_0–W_t)/(W_0–W_\infty)$) *versus* time. W_0 is the initial weight of the cast film plus the glass plate at time 0, W_t is the weight at time t and W_∞ is the final weight, when the solvent is completely evaporated. The following empirical equation was proposed to describe solvent evaporation during the early stage of the dry step for membrane formation by the dry/wet phase inversion method [53]:

$$\frac{W_0-W_t}{W_0-W_\infty} = 1 - \exp\left(-bt^m\right) \quad (5)$$

where b is an empirical parameter indicating how sooner the solvent starts to evaporate while m represents the rate of solvent evaporation.

Table 4 presents the obtained empirical parameters (m and b) of the spinning solutions prepared with different solvents. The reasonably good linear fit in Fig. 5 indicates that Eq. (5) is suitable to describe the solvent evaporation during the early stage of the dry step for hollow fiber membrane formation. It can be seen that when the quantity of TMP in the solvents mixture was increased the parameter m decreased indicating a reduction of the solvent evaporation rate. However, no significant changes

were detected for the parameter *b* concluding that the amount of TMP in the solvents mixture did not affect the onset time of solvent evaporation. Castellari and Ottani [54] stated that the mass transfer within the polymeric cast film, during the solvent evaporation step, was a combination of both solvent diffusion and polymer contraction. Taking into consideration that the diffusion coefficient (D_m in Table 3) of TMP is lower than that of DMAC, the lowest *m* value was obtained for the DMAC40 cast film prepared with the highest amount of TMP (see Table 4). When DMF was used as solvent instead of DMAC, the parameter *b* for the spinning solution DMF60 was found to be greater than that for the solution DMAC60, resulting in a quick initial solvent evaporation time when using DMF. This may be attributed partly to the lower boiling point of DMF (153ºC) compared to that of DMAC (165ºC) or which is the same the higher vapor pressure of the solvent DMF.

The dynamics of wet phase inversion was characterized by the solvent/nonsolvent exchange rate, which could give information on the structural morphology of the membrane. Faster solvent/nonsolvent exchange rate promotes the formation of finger-like structure or even macro-voids.. Figure 6 illustrates the demixing curves of the studied spinning solutions by light transmittance. As it can be seen in Fig. 6, the phase inversion kinetic of the PVDF-HFP spinning solutions showed three stages. The normalized transmittance decreased slowly in the first stage, then it is quickly decreased in the second stage and finally it reduced slightly in the third stage approaching an asymptotic transmittance value. The same trend was observed previously by Li et al. [39,40]. The first stage indicated a delay of the nonsolvent (water) penetration in the cast PVDF-HFP film. This effect can be attributed to the hydrophobic nature of this copolymer that delays the penetration of water during phase separation process [41]. However, no full delay was observed because the normalized transmittance did not

maintain the same value to unity but it declined to approximately 0.8 attributed to the presence of the hydrophilic polymer, PEG, in the spinning solution. For this reason, this period was termed the first stage instead of “time lag”. Lang et al. [55] also observed this effect when a hydrophilic polymer, perfluorosulfonic acid (PFSA), was added in the PVDF/DMAC solution. A perfect delayed demixing curve with its time lag period was obtained when PFSA was not added in the PVDF/DMAC solution.

The registered period of the first stage increased with the use of the solvent DMAC and with the increase of TMP amount in the solvents mixture (DMAC/TMP). Moreover, it can be seen in Fig. 6 that the demixing rate declined with the increase of the amount of TMP in the solvents mixture. In addition, the coagulation rate of the spinning solution prepared with DMF (DMF60) was found to be the highest. These coagulation kinetic experiments agreed well with the solvent diffusion coefficients (Table 3) and the viscosity of the spinning solutions (Table 1). The highest diffusion coefficient corresponds to the solvent DMF, whereas the smallest one is for the solvent TMP. These mean a faster exchange rate between water and DMF and a slower water-solvent exchange when TMP was employed. As it was stated earlier, the coagulation rate also depends strongly on the viscosity of the spinning solutions. The more viscous is the spinning solution, the lower is the PVDF-HFP coagulation rate. This effect has been observed when increasing the TMP amount in the solvent mixture and when changing DMF by DMAC. The solubility parameter difference and the thermodynamic results were both related with the initiation of the PVDF-HFP coagulation process, being able to conclude that the use of DMF and the increase of the TMP concentration in the solvent mixture may result in an earlier PVDF-HFP precipitation because less quantity of water was required (i.e. lower cloud point, Fig. 3).

3.2 Hollow fiber membrane characterization

3.2.1 Effects of the solvent(s) on the internal structure of the PVDF-HFP hollow fibers

The cross-sectional structure of the PVDF-HFP hollow fiber membranes were studied by SEM. Figure 7 shows the evolution of the cross-section structure of the hollow fiber membranes depending on the type of the used solvent(s). All membranes exhibit a common overall structure, which is a sponge-like structure in the middle layer and a finger-like structure in the internal and external layers of the hollow fiber membranes. The observed SEM membrane morphology confirms that the hollow fibers were formed by nucleation of the copolymer lean phase resulting in a porous structure. Larger and longer tear-drop macro-voids between the inner layer and sponge-like structure in the middle layer can be observed in the hollow fibers prepared with the mixture of the solvents DMF/TMP. These macro-voids disappeared in the middle layer of the hollow fiber membranes when DMAC was used instead DMF in the solvent mixtures. In the case of flat sheet PVDF membranes prepared with different solvents mixtures, Li et al. [39] also observed that the increase of the solubility parameter difference between the polymer and the solvent, the weaker solvent power, the lower cloud point and the higher viscosity, lead to a slow polymer coagulation rate and avoid the formation of macro-voids and finger-like structures. Macro-voids can also be reduced to parallel finger-like structure or disappear and even turn to sponge-like structure with the increase of the copolymer concentration in the spinning solution [28]. It is worth noting that, in general the formation of macro-voids is an undesirable structure for MD [6,12,56]. Macro-voids can cause a weak mechanical strength, facilitate pore wetting and therefore reduce the long-term use of the membrane. For long-term performance application it is better to use membranes exhibiting a sponge-like structure through its cross-section [1,12,13]. When the TMP content in DMAC was

increased, the sponge-like structure in the middle layer became thicker, whereas the finger-like structure formed at the outer side of the hollow fiber prepared with DMAC/TMP was decreased. Furthermore, the finger-like structure of the internal layer became slightly longer and narrower with the increase of TMP rate in the solvent mixture DMAC/TMP.

The observed changes of the structural morphology of the PVDF-HFP hollow fiber membranes can be associated to the previously reported characteristics of the spinning solutions based on the solubility parameters, thermodynamic tests, viscosity, coagulation rate and evaporation kinetic experiments. Elimination of macro-voids from the cross-section structure may be due to the increase of the viscosity of the spinning solution when using DMAC solvent instead of DMF (DMF60 and DMAC60 in Table 1). It has been demonstrated that increasing the dope viscosity is the main approach to suppress macro-voids from the cross-section of phase inversion membranes [56]. Furthermore, based on the calculated R_{HSP} (*P*-*S*) values, the best solvent is DMAC; whereas based on the calculated R_{HSP} (*W*-*S*) values, the highest solvent-water affinity corresponds to the spinning solution prepared with DMF. Therefore, the solvent DMF has less affinity towards the copolymer PVDF-HFP and better affinity to water than DMAC, facilitating in this case the interdiffusion between water and the solvent(s) during hollow fiber coagulation. The PVDF-HFP coagulation rate is faster and earlier when the solvent DMF was used as solvent, as it can be predicted also from the coagulation kinetics (see Fig. 6) and from the evaporation kinetics (see parameter *b* in Table 4) and the thermodynamic results (see Fig. 3), respectively. These lead to the formation of bigger fingers in the inner layer ended by macro-voids inside the cross-section as can be seen in Fig. 7 for the membrane DMF60.

Among all the PVDF-HFP spinning solutions considered in this study (see Table 1), the one prepared with the solvent mixture DMAC/TMP with the maximum TMP content in DMAC has the highest viscosity. Therefore, by increasing the TMP ratio in the solvent mixture, both the viscosity of the spinning solution and the R_{HSP} (*P-S*) increased and the cloud point declined affecting the kinetics of the phase inversion during membrane formation process. As a result, a larger sponge-like structure was obtained for higher TMP ratio.

The observed longer and narrower finger-like structure of the internal layer with the increase of TMP concentration in the dope solution can be due to the cloud point reduction (Fig. 3) and the increase of R_{HSP} (P-S) (Table 3). The lower coagulation (i.e. cloud point) and the higher R_{HSP} (P-S) both induced a deeper nonsolvent diffusion to the spinning solution and an easier solvent extraction from the spinning solution.

The SEM images were analyzed by UTHSCSA ImageTool 3.0 to determine the thickness of the finger-like and sponge-like structures of the different layers. The sponge-like structure in the middle layer represents 27%, 43% and 53% of the total thickness of the hollow fiber membranes DMAC100, DMAC60 and DMAC40, respectively. As it has been mentioned earlier, a macro-void free structure is desirable in membrane processes. Therefore, the membranes DMAC60 and DMAC40 exhibited better structure than the other prepared hollow fiber membranes with similar materials PVDF-HFP/PEG/DMAC, having cross-section structures containing a high percentage area covered by macro-voids (i.e. 63 - 76%) [20].

For PVDF polymer, Li et al. [39,40] observed a delayed demixing hindering the development of finger-like structure when using the solvents mixture having the poorest solvent power. Similar result is obtained in this study when increasing the amount of

TMP in the in the solvent mixture (DMAC/TMP) (i.e. increase of R_{HSP} (P-S)). In addition, a weaker solvent power and a higher solution viscosity mainly enhanced the shrinkage of the membranes [39]. The areas of the membranes were measured before and after the evaporation test, obtaining reductions of their areas of (i.e. shrinkage) of 32%, 35% and 41% for DMAC100, DMAC60 and DMAC40, respectively. Higher shrinkage of the membranes and lower solvent evaporation rate (see the parameter *m* in Table 4) resulted in denser and more wrinkled skin-layer [17], which acted as a resistive barrier between the coagulation bath and the interior region of the membrane [57]. Consequently, a delayed demixing was detected with the increase of TMP amount in the solvents mixture (i.e. first stage period of the coagulation curves in Fig. 6 became longer) and the thickness of the finger-like structure of the external layer of the hollow fiber membranes decreased. The finger like structure layer of the external surface represents 34%, 19% and 6% of the total thickness of the hollow fiber membranes for DMAC100, DMAC60 and DMAC40, respectively.

3.2.2 Effects of the solvent(s) on the morphological characteristics of the PVDF-HFP hollow fibers

The internal and external diameters as well as the thickness of the prepared PVDF-HFP hollow fiber membranes are summarized in Table 5. No clear trends were detected for the effects of TMP content on both the thickness and the diameters, which were not changed significantly. Among all PVDF-HFP hollow fiber membranes, DMAC60 is the thinnest one. The thickness of all prepared hollow fiber membranes are thicker than those prepared under similar spinning conditions in our previous study [28]. For example, if the membrane DMAC100 is compared to the membrane CO19 (PVDF-HFP (19 wt.%)/PEG (3 wt.%)/ DMAC) in [28], it can be seen a decrease in both the inner and outer diameters and an increase of the thickness (more than two times). This can be

attributed to the higher amount of PEG used in this study, 5 wt.% instead of 3 wt.%, as described elsewhere [26]. The thickness enhancement may be attributed to the viscosity of the dope solution, which increased with increasing PEG concentration in the dope solution (i.e. increase of the shear stress of the dope solution within the spinneret).Both the inner and outer diameters as well as the thickness of the PVDF-HFP hollow fiber membrane prepared with DMF (DMF60) were greater than those of the membrane prepared with DMAC (DMAC60). These results may be attributed to the surface tension of the spinning solution, which is higher for DMF/TMP (DMF60) compared to DMAC/TMP (DMAC60). Moreover, the higher thickness of the membrane DMF60 compared to the membrane DMAC60 can also be explained admitting that the same quantity of copolymer is more closely packed in a spongy structure than in an asymmetric structure containing macro-voids [59-61].

The void volume fraction (ε) of the hollow fiber membranes is shown in Table 5. No clear trend was detected for the void volume fraction in relation with the TMP content in the solvent mixture, and the membranes DMAC100 and DMAC40 exhibited the highest void volume fraction values. Similar ε values were reported in previous studies for of PVDF and PVDF-HFP hollow fiber membranes [6,8,14,28]. However, the ε values obtained in this study are higher than those presented by Khayet et al. [20,42] for PVDF (lower than 43%) and PVDF-HFP (lower than 60%) hollow fiber membranes.

The measured *LEP* values of the hollow fiber membranes are also shown in Table 5. These *LEP* values are greater than those reported by Khayet el al. [20] for PVDF-HFP hollow fiber membranes, which are between 0.25 and 0.75 10^5 Pa, and lower *LEP* values than the majority of PVDF hollow fiber membranes prepared by Khayet et al. [42]. The highest *LEP* value in this study was obtained for the membrane DMAC100 and it is similar to those obtained by García-Payo et al. [28] when it is compared with

the same PVDF-HFP concentration and the same single solvent DMAC (CO19 membrane in [28]). Therefore, among all prepared PVDF-HFP hollow fiber membranes it may be expected a small maximum pore size of this membrane. For the membranes prepared with TMP mixed solvent (DMAC40, DMAC60 and DMF60), the *LEP* value decreased by half that of DMAC100.

The SEM image of the cross-section of the membrane DMF60 showed macro-voids in the middle layer. The formation of these macro-voids could facilitate membrane wetting, decreasing the corresponding *LEP* value. The lower *LEP* of the hollow fiber membranes prepared with the mixed solvent DMAC/TMP (DMAC60 and DMAC40) compared to that of DMAC10 may be attributed to the main difference observed for the external layer structure. DMAC100 had longer and bigger fingers, while the membranes DMAC60 and DMAC40 had shorter and narrower fingers in their external layer. The finger-like structure of the outer surface of the membrane DMAC100 may hinder the exit of the wetting liquid and therefore it is necessary to apply more hydrostatic pressure before water flows out of this membrane. On the other hand, the *LEP* values of the membranes DMAC60 and DMAC40 are almost similar and lower than that of DMAC100, due to the shorter and narrower fingers of the outer structure. In general, judging from the obtained *LEP* values, all prepared membranes in this study can be used in MD.

Figures 8 and 9 show the 3D AFM images of the inner and outer surfaces of the PVDF-HFP hollow fiber membranes, respectively. AFM images reveal that the surfaces of all membranes possess smooth nodule-like and valley-like structures. The bright peaks represent nodules and the dark depressions (i.e. valleys) are pores. 3D AFM images also permit to estimate the roughness of both the internal and external surfaces of the membranes. The obtained mean roughness parameters (minimum, maximum and

average values) are summarized in Table 6, being all the values similar to those of other hollow fiber membranes [20,26,28,42]. The mean roughness of both the inner and outer surfaces decreased when DMF (DMF60) was used instead DMAC (DMAC60). Moreover, the mean roughness of the internal surfaces of the membranes DMF60 and DMAC60 was similar to the mean roughness of their external surfaces. It is worth noting that no clear trend was detected between the mean roughness of the inner surfaces and the increase of the TMP content in the solvent mixture. This may be due to the slight change in the R_{HSP} values for the pair *W-S*. However, an increase of TMP concentration results in a small and gradual enhancement of the mean roughness of the outer surfaces. As it was stated previously, this effect can be related to the shrinkage of the membrane, which enhanced with the increase of the TMP amount in the solvent mixture. A higher shrinkage of the membranes resulted in dense and wrinkled surface [17] and consequently a rougher outer surface of the hollow fiber membranes.

The mean pore sizes and their corresponding geometric standard deviations of both the inner and outer surfaces of the hollow fibers are summarized in Table 7. The mean pore sizes of the surfaces of other PVDF-HFP and PVDF hollow fiber membranes were found to be similar or even greater than the values of the membranes prepared in this study [20,26,28,42]. Figures 10 and 11 show the cumulative pore size distributions and the probability density function curves. The pore size distributions of the internal and external surfaces (Figs. 10 and 11) of the membranes prepared with mixed solvents (DMAC/TMP or DMF/TMP) were found to be narrower than those of the hollow fibers fabricated with a single solvent, DMAC (membrane DMAC100). It was observed a slight increase of the mean pore size of the external surfaces of the hollow fibers when TMP content in the solvent mixture was increased. This result may be attributed partly to the decrease of the solvent(s) evaporation rate, which increases the pore size of the

outer membrane surface. Among all prepared hollow fibers the smallest mean roughness and mean pore size of the outer surface correspond to the membrane DMF60. When comparing the membranes DMAC60 and DMF60, the observed smaller mean pore size and mean roughness of the membrane DMF60 may be explained based on the high value of its parameter *b* (see Table 4) and the lowest observed shrinkage (i.e. 26%) from the solvent evaporation kinetic results, indicating an earlier solvent evaporation and the subsequent formation of a thicker and smoother skin-layer. By changing the solvent DMAC to DMF, no clear tendency was found for the pore sizes of the inner surfaces of the hollow fiber membranes. The mean pore size decreased and then increased with the TMP content in the solvents. The membrane DMAC60 exhibited the smallest mean pore size.

The mean pore sizes (r_p) obtained from the wet curve (Porometry method) and the dry curve (gas permeation method) together with the effective porosity (ε/L_p) of the PVDF-HFP hollow fiber membranes are summarized in Table 8. Because of the low mechanical properties of the membrane DMF60 having large and long tear-drop macro-voids, these tests cannot be carried out using this membrane. Taking into account the standard deviation, the mean pore sizes determined by the two methods are quite similar for all PVDF-HFP hollow fiber membranes. Moreover, it can be seen a greater mean pore size for the hollow fiber membrane prepared with higher TMP content in the solvents mixture. However, the lowest effective porosity was found for the hollow fiber membrane prepared with the highest TMP concentration in the solvents mixture. It is worth quoting that the effective porosity reported by Tang et al. [14] for PVDF hollow fiber membranes prepared with the solvent DMAC are similar to those presented in Table 8.The thermal properties of the PVDF-HFP hollow fiber membranes were studied by DSC and the obtained thermograms are presented in Fig. 12. Table 9 summarizes the

melting temperature (T_m), the crystallization temperature (T_c), the enthalpy of melting (ΔH_m) and the enthalpy of crystallization (ΔH_m). In general, if the standard deviations are taking into consideration, all the obtained transition peaks of the membranes as well as T_m, T_c, ΔH_m and ΔH_m are almost similar to those of the copolymer PVDF-HFP. It was observed that the crystallinity of the studied PVDF-HFP hollow fiber membranes is lower than that of the PVDF hollow fiber membranes, which is in the range 40-50% [18,38,41]. Moreover, the obtained crystallinity values in this study agree with those obtained by Tian et al. [58] for flat sheet PVDF-HFP membranes prepared with DMAC or acetone. Providing that both T_m and T_c of the PVDF-HFP hollow fiber membranes are much higher than the DCMD operating temperatures, these membranes will maintain their thermal stability during DCMD processing.

3.3 DMCD performance

The DMCD performance of the fabricated hollow fibers with different solvents was carried out as stated previously. Distilled water and NaCl aqueous solution (3 wt.%) were used as feed. As it was expected the permeate flux (J) of all membranes increased exponentially, following an Arrhenius type of dependence, with the feed temperature (T_{feed}). Figure 13 shows as an example the DCMD permeate flux of the PVDF-HFP hollow fiber membranes (DMF60) as a function of different feed temperatures maintaining the permeate temperature at 25ºC. In addition, as it is well known in MD, when the salt solution (3 wt.%) was used as feed the permeate fluxes are lower than the permeate flux obtained for feed distilled water. For sake of comparison, Figure 14 shows the permeate fluxes of all hollow fiber membranes prepared with different solvents. The obtained DCMD permeate fluxes are similar to those of other PVDF-HFP hollow fiber membranes [20,26]. As it can be seen in Fig. 14, the type of solvent affects the characteristics of the PVDF-HFP hollow fiber membranes and their DCMD

permeate flux as a consequence. The hollow fiber membrane (DMAC60) prepared with the solvent DMAC exhibited higher DCMD permeate flux than the membrane (DMF60) prepared with the solvent DMF. As it is discussed previously, compared to the membrane DMF60, the membrane DMAC60 exhibits thicker internal sponge-like structure with fewer macro-voids (see Fig. 7), lower thickness, higher mean roughness of both the outer and inner surfaces and similar porosity. These justify the higher DCMD permeate flux of the membrane DMAC60 compared to the membrane DMF60. On the other hand, DCMD permeate flux was increased with increasing TMP concentration in the solvent mixture, due the formation of a thicker sponge-like structure in the membrane cross-section, a higher mean roughness of the external surface and a bigger mean pore size. Larger mean pore size usually corresponds to higher permeate flux [6].

The permeate flux reduction factor (*FRF*) represents the permeate flux difference when the salt aqueous solution (J_{NaCl}) was used as feed instead of distilled water (J_w) and defined as:

$$FRF\ (\%) = \frac{(J_w - J_{NaCl})}{J_w} \times 100 \qquad (6)$$

The highest *FRF* value corresponds to the membrane DMF60 (33,5%) whereas the lowest *FRF* value was obtained for the membrane DMAC40 (17,5%). A quality membrane must exhibit a high desalination performance with a low *FRF*. When changing DMF by DMAC in the solvent mixture, the *FRF* value decreased due partly to the increase of both the internal and external mean roughness, which reduced the concentration polarization effect. All the above indicated results corroborate that DMAC is better solvent than DMF for the preparation of PVDF-HFP hollow fiber membranes. Another parameter that must be taken into account is the salt rejection

factor. The obtained values were 99.65, 99.30, 99.80, 99.35% for DMF60, DMAC100, DMAC60, DMAC40, respectively. The highest salt rejection factor was achieved for the membrane DMAC60, which corresponds to the lowest mean pore size of the inner surface.

4. Conclusions

The type of solvent affects both the characteristics and the DCMD permeate flux of the PVDF-HFP hollow fiber membrane prepared by the dry/wet spinning technique. By choosing an adequate solvent or solvents mixture with the aid of the results obtained by the different spinning solutions characterization techniques the internal structure of the hollow fiber membrane may be predicted for preparation of a high MD membrane performance.

The type of the used solvent(s) completely changed the spinning solution characteristics. The selected solvent modified the solvent-copolymer-nonsolvent interaction and consequently dictated the kinetic and the thermodynamic precipitation of the membrane formation. These affected the morphological characteristics of the hollow fiber membranes and the MD performance. The thicker the sponge-like structure of the hollow fiber membrane, the higher the MD permeate flux is.

Macro-voids disappeared from the cross-section of the hollow fiber membranes when DMAC was used instead DMF because DMAC is better solvent for PVDF-HFP than DMF. DMAC leads to higher viscosity, thermodynamic stability and lower coagulation rate. The onset time of the solvent evaporation clearly decreased when DMAC was used instead DMF rendering the external layer less dense with higher mean roughness and greater outer surface mean pore size. When the solvent was changed

from DMF to DMAC, both the DCMD permeate flux and the salt (NaCl) rejection factor were enhanced because of the thicker internal sponge-like structure, the lower thickness and the higher mean roughness of both the outer and inner surfaces.

The hollow fibers prepared with the mixed solvents, DMF/TMP and DMAC/TMP in this study, exhibited narrow pore size distributions but low *LEP* results.

When the TMP concentration in the solvents mixture was increased, the affinity between PVDF-HFP and the solvent(s) decreased, whereas the viscosity of the spinning solutions was increased. Furthermore, the solvent(s) evaporation rate and the coagulation rate of PVDF-HFP became slow and the thickness of the finger-like structure of the external layer was reduced (i.e. formation of a thicker sponge-like structure in the membrane cross-section). Higher mean roughness of the external surface and greater mean pore sizes were obtained when the TMP amount in the solvent mixture was higher. These results lead to higher DCMD permeate fluxes for the PVDF-HFP hollow fiber membranes prepared with more amount of TMP in the solvents mixture. The solvent DMAC was found to be better solvent than DMF and the increase of TMP content enhanced the desalination performance of the PVDF-HFP hollow fiber membrane.

Acknowledgements

The authors acknowledge the financial support of the Spanish Ministry of Science and Innovation I+D+I Project MAT2010-19249. L. García-Fernández is thankful to the Spanish Ministry of Education, Culture and Sport (MECD) for the FPU grant.

References

[1] M. Khayet, T. Matsuura, Membrane Distillation. Principles and Aplications, Elsevier (2011).

[2] M. Khayet, Membranes and theoretical modeling of membrane distillation: A review, Adv. Colloid Interface Sci. 164 (2011) 326–339.

[3] M. Gryta, M. Barancewicz, Influence of morphology of PVDF capillary membranes on the performance of direct contact membrane distillation, J. Membr. Sci. 358 (2010) 158–167.

[4] L. Song, B. Li, K. Sirkar, J. Gilron, Direct contact membrane distillation-based desalination: novel membranes, devices, larger-scale studies, and a model, Ind. Eng. Chem. Res. 46 (8) (2007) 2307–2323.

[5] M. Essalhi, M. Khayet, Surface segregation of fluorinated modifying macromolecule for hydrophobic/hydrophilic membrane preparation and application in air gap and direct contact membrane distillation, J. Membr. Sci. 417–418 (2012) 163–173.

[6] M.M. Teoh, T.S. Chung, Membrane distillation with hydrophobic macrovoid-free PVDF–PTFE hollow fiber membranes, Sep. Purif. Technol. 66 (2009) 229–236.

[7] M.C. García-Payo, M. Essalhi, M. Khayet, Preparation and characterization of PVDF–HFP copolymer hollow fiber membranes for membrane distillation, Desalination, 245 (2009) 469-473.

[8] D.Y. Hou, J. Wang, D. Qu, Fabrication and characterization of hydrophobic PVDF hollow fiber membranes for desalination through direct contact membrane distillation, Sep. Purif. Technol. 69 (2009) 78–86.

[9] K.Y. Wang, T.S. Chung, M. Gryta, Hydrophobic PVDF hollow fiber membranes with narrow pore size distribution and ultra-thin skin for the fresh water production through membrane distillation, Chem. Eng. Sci. 63 (2008) 2587–2594.

[10] X. Yang, R. Wang, L. Shi, A.G. Fane, M. Debowski, Performance improvement of PVDF hollow fiber-based membrane distillation process, J. Membr. Sci. 369 (2011) 437–447.

[11] P. Wang, M.M. Teoh, T.S. Chung, Morphological architecture of dual-layer hollow fiber for membrane distillation with higher desalination performance, Water Res. 45 (17) (2011) 5489–5500.

[12] C.Y. Feng, K.C. Kulbe, T. Matsuura, A.F. Ismail, Review. Recent progresses in polymeric hollow fiber membrane preparation, characterization and applications, Sep. Puri. Tech. 111 (2013) 43–71.

[13] N. Peng, N. Widjojo, P. Sukitpaneenit, M.M. Teoh, G.G. Lipscomb, T.S. Chung, J.Y. Lai, Evolution of polymeric hollow fibers as sustainable technologies: past, present and future, Prog. Polym. Sci. 37 (2012) 1401–1424.

[14] Y. Tang, N. Li, A. Liu, S. Ding, C. Yi, H. Liu, Effect of spinning conditions on the structure and performance of hydrophobic PVDF hollow fiber membranes for membrane distillation, Desalination 287 (2012) 326–339.

[15] M. Khayet, The effects of air gap length on the internal and external morphology of hollow fiber membranes, Chem. Eng. Sci. 58 (2003) 3091–3104.

[16] M. Khayet, M.C. García-Payo, F.A. Qusay, K.C. Khulbe, C.Y. Feng, T. Matsura, Effects of gas gap type on structural morphology and performance of hollow fibers, J. Membr. Sci. 311 (2008) 259–269.

[17] X.Y. Wang, L. Zhang, D.H. Sun, Q.F. An, H.L. Chen, Effect of coagulation bath temperature on formation mechanism of poly(vinylidene fluoride) membrane, J. Appl. Polym. Sci. 110 (2008) 1656–1663.

[18] S.H. Choi, F. Tasselli, J.C. Jansen, G. Barbieri, E. Drioli, Effect of the preparation conditions on the formation of asymmetric poly(vinylidene fluoride) hollow fibre membranes with a dense skin, J. Eur. Polym. 46 (2010) 1713–1725.

[19] X. Yang, H. Yu, R. Wang, A.G. Fane, Optimization of microstructured hollow fiber design for membrane distillation applications using CFD modeling, J. Membr. Sci. 421–422, (2012) 258–270.

[20] M. Khayet, C. Cojocaru, M. Essalhi, M.C. García-Payo, P. Arribas, L. García-Fernández, Hollow fiber spinning experimental design and analysis of defects for fabrication of optimized membranes for membrane distillation, Desalination 287 (2012) 146–158.

[21] C.S. Feng, B.L. Shi, G.M. Li, Y.L. Wu, Preparation and properties of microporous membrane from poly(vinylidene fluoride-co-tetrafluoroethylene) (F2.4) for membrane distillation, J. Membr. Sci. 237 (2004) 15–24.

[22] L. Shi, R. Wang, Y. Cao, D.T. Liang, J.H. Tay, Effect of additives on the fabrication of poly(vinylidene fluoride-co-hexafluropropylene) (PVDF-HFP) asymmetric microporous hollow fiber membranes, J. Membr. Sci. 315 (2008) 195–204.

[23] L. Shi, R. Wang, Y. Cao, C. Feng, D.T. Liang, J.H. Tay, Fabrication of poly(vinylidene fluoride-co-hexafluropropylene) (PVDF-HFP) asymmetric microporous hollow fiber membranes, J. Membr. Sci.305 (2007) 215–225.

[24] C. Feng, R. Wang, B. Shi, G. Li, Y. Wu, Factors affecting pore structure and performance of poly(vinylidene fluoride-co-hexafluoropropylene) asymmetric porous membrane, J. Membr. Sci.277 (2006) 55–64.

[25] G.C. Li, P. Zhang, H.P. Zhang, L.C. Yang, Y.P. Wu, A porous polymer electrolyte based on P(VDF-HFP) prepared by a simple phase separation process, Electrochem. Comm. 10 (2008) 1883–1885.

[26] M.C. García-Payo, M. Essalhi, M. Khayet, L. García-Fernández, K. Charfi, H. Arafat, Water desalination by membrane distillation using PVDF-HFP hollow fiber membranes, Membrane Water Treatment 1 (2010) 215–230.

[27] L. Shi, R. Wang, Y. Cao, Effect of the rheology of poly(vinylidene fluoride co-hexafluropropylene) (PVDF-HFP) dope solutions on the formation of microporous hollow fibers used as membrane contactors, J. Membr. Sci. 344 (2009) 112–122.

[28] M.C. García-Payo, M. Essalhi, M. Khayet, Effects of PVDF-HFP concentration on membrane distillation performance and structural morphology of hollow fiber membranes, J. Membr. Sci. 347 (2010) 209–219.

[29] J.H. Cao, B.K. Zhu, Y.Y. Xu, Structure and ionic conductivity of porous polymer electrolytes based on PVDF-HFP copolymer membranes, J. Membr. Sci. 281 (2006) 446–453.

[30] Y.J. Hwang, S.K. Jeong, K.S. Nahm, A.M. Stephan, Electrochemical studies on poly(vinylidene fluoride-hexafluoropropylene) membranes prepared by phase inversion method, Eur. Polym. J. 43 (2007) 65–71.

[31] S. Wongchitphimon, R. Wang, R. Jiraratananona, L. Shi, C.H. Loh, Effect of polyethylene glycol (PEG) as an additive on the fabrication of polyvinylidene fluoride-co-hexafluropropylene (PVDF-HFP) asymmetric microporous hollow fiber membranes, J. Membr. Sci. 369 (2011) 329–338.

[32] P. van de Witte, P.J. Dijkstra, et al., Phase separation processes in polymer solutions in relation to membrane formation, J. Membr. Sci. 117 (1996) 1–31.

[33] Z. Song, M. Xing, J. Zhang, B. Li, S. Wang, Determination of phase diagram of a ternary PVDF/γ-BL/DOP system in TIPS process and its application in preparing hollow fiber membranes for membrane distillation, Sep. Puri. Tech. 90 (2012) 221–230.

[34] A.C. Sun, W. Kosar, Y. Zhang, X. Feng, A study of thermodynamics and kinetics pertinent to formation of PVDF membranes by phase inversion, Desalination 309 (2013) 156–164.

[35] A. Mansourizadeh, A.F. Ismail, Preparation and characterization of porous PVDF hollow fiber membranes for CO_2 absorption: Effect of different non-solvent additives in the polymer dope, Int. J. Greenh. Gas Control 5 (2011) 640–648.

[36] M.L. Yeow, Y.T. Liu, K. Li, Isothermal Phase Diagrams and Phase-Inversion Behavior of Poly(vinylidene fluoride)/Solvents/Additives/Water Systems, J. Appl. Polym. Sci. 90 (2003) 2150–2155.

[37] M.L. Yeow, Y.T. Liu, K. Li, Morphological Study of Poly(vinylidene fluoride) Asymmetric Membranes: Effects of the Solvent, Additive, and Dope Temperature, J. Appl. Polym. Sci. 92 (2004) 1782–1789.

[38] Y.K. Ong, N. Widjojo, T.S. Chung, Fundamentals of semi-crystalline poly(vinylidene fluoride) membrane formation and its prospects for biofuel (ethanol and acetone) separation via pervaporation, J. Membr. Sci. 378 (2011) 149–162.

[39] Q. Li, Z.L. Xu, L.Y. Yu, Effects of Mixed Solvents and PVDF Types on Performances of PVDF Microporous Membranes, J. Appl. Polym. Sci. 115 (2010) 2277–2287.

[40] Q. Li, Z.L. Xu, M. Liu, Preparation and characterization of PVDF microporous membrane with highly hydrophobic surface, Polym. Adv. Technol. 22 (2011) 520–531.

[41] Y.K. Ong, T.S. Chung, High performance dual-layer hollow fiber fabricated via novel immiscibility induced phase separation (I^2PS) process for dehydration of ethanol, J. Membr. Sci., 421-422 (2012) 271–282.

[42] M. Khayet, C. Feng, K.C. Khulbe, T. Matsuura, Preparation and characterization of polyvinylidene fluoride hollow fiber membranes for ultrafiltration, Polymer 43 (2002) 3879–3890.

[43] M.C. García-Payo, M.A. Izquierdo-Gil, C. Fernández-Pineda, Wetting study of hydrophobic membranes via liquid entry pressure measurements with aqueous alcohol solutions, J. Colloid Interface Sci. 230 (2002) 420–431.

[44] M. Essalhi, M. Khayet, Self-sustained webs of polyvinylidene fluoride electrospun nanofibers at different electrospinning times: 1. Desalination by direct contact membrane distillation, J. Membr. Sci., 433 (2013) 167-179].

[45] X. Tian, X. Jiang, Poly (vinylidene fluoride-co-hexafluoropropene) (PVDF-HFP) membranes for ethyl acetate removal from water, J. Hazard. Mater. 153 (2008) 128–135.

[46] M. Tazaki, R. Wada, M. Okabe, T. Homma, Crystallization and gelation of poly (vinylidene fluoride) in organic solvents, J. Appl. Polym. Sci. 65 (8) (1997) 1517–1524.

[47] C.M. Hansen, Hansen solubility parameters: a user´s handbook. 2nd ed. CRC Press, Taylor & Francis Group (2007).

[48] S. Abbott, C.M. Hansen, H. Yamamoto, Hansen Solubility Parameters in Practice - Complete with software, data, and examples, 3rd ed. Ebook: Hansen-solubility.com (2010).

[49] J.E. Mark (Ed.), Polymer Data Handbook, Oxford University Press (1999).

[50] N. Widjojo, T.S. Chung, D.Y. Arifin, M. Weber, V. Warzelhan, Elimination of die swell and instability in hollow fiber spinning process of hyperbranched polyethersulfone (HPES) via novel spinneret designs and precise spinning conditions, Chem. Eng. J. 163 (2010) 143-153.

[51] C.C. Pereira, R. Nobrega, C.P. Borges, Spinning process variables and polymer solution effects in the die-swell phenomenon during hollow fiber membranes formation, Brz. J. Chem. Eng. 17 (2000) 4–7.

[52] A. Bottino, G. Camera-Roda, G. Capannelli, S. Munari, The formation of microporous polyvinylidenedifluoride membranes by phase separation, J. Membr. Sci. 57 (1) (1991) 1–20.

[53] R.Y.M. Huang, X. Feng, Studies on solvent evaporation and polymer precipitation pertinent to the formation of asymmetric polyetherimide membranes, J. Appl. Polym. Sci. 57 (1995) 613–621.

[54] C. Castellari, S. Ottani, Preparation of reverse osmosis membranes. A numerical analysis of asymmetric membrane formation by solvent evaporation from cellulose acetate casting solutions, J. Membr. Sci. 9 (1981) 29–41.

[55] W.Z. Lang, Z.-L. Xu, H. Yang, W. Tong, Preparation and characterization of PVDF-PFSA blend hollow fiber UF membrane, J. Membr. Sci. 288 (2007) 123-131.

[56] N. Peng, T.S. Chung, K.Y. Wang, Macrovoid evolution and critical factors to form macrovoid-free hollow fiber membranes, J. Membr. Sci. 318 (2008) 363–372.

[57] A.F. Ismail, L. P. Yean, Review on the development of defect-free and ultrathin-skinned asymmetric membranes for gas separation through manipulation of phase inversion and rheological factors, J. Appl. Polym. Sci. 88 (2003) 442-451.

[58] X. Tian, X. Jiang, B. Zhu, Y. Xu, Effect of the casting solvent on the crystal characteristics and pervaporative separation performances of P(VDF-*co*-HFP) membranes, J. Membr. Sci. 279 (2006) 479–486.

[59] N. Vogrin, C. Stropnik, V. Musil, M. Brumen, The wet phase separation: the effect of cast solution thickness on the appearance of macrovoids in the membrane forming ternary cellulose/acetone/water system, J. Membr. Sci. 207 (2002) 139-141.

[60] D. Li, T.S. Chung, J. Ren, R. Wang, Thickness dependence of macrovoid evolution in wet phase-inversion asymmetric membranes, Ind. Eng. Chem. Res. 43 (2004) 1553-1556.

[61] N. Widjojo, T.S. Chung, Thickness and air gap dependence of macrovoid evolution in phase-inversion asymmetric membranes, Ind. Eng. Chem. Res. 45 (2006) 7618-7626.

FIGURES

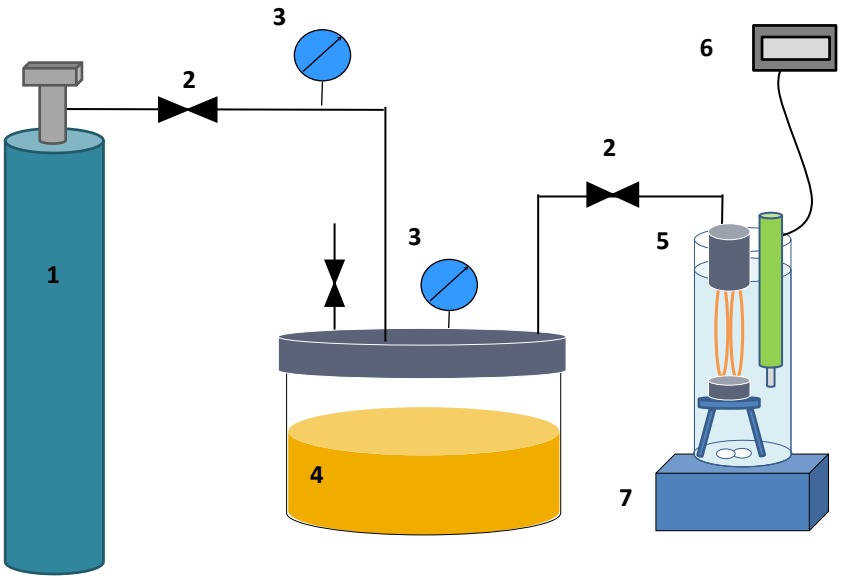

Figure 1. Experimental *LEP* set-up for salt aqueous solutions. (1) Nitrogen tank; (2) regulating pressure valve; (3) pressure gauge; (4) salt solution vessel; (5) hollow fiber module; (6) electrical conductivity meter; (7) magnetic stirrer.

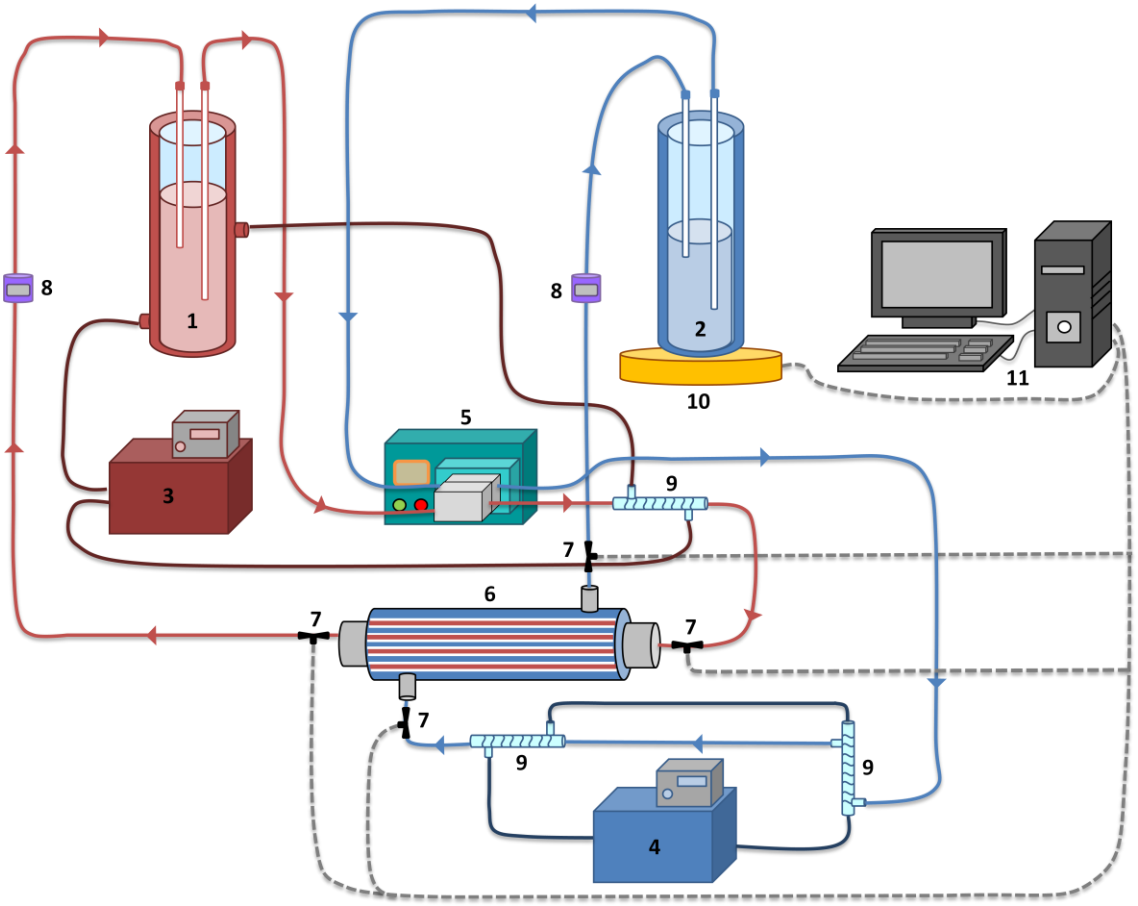

Figure 2. Experimental set-up for direct contact membrane distillation (DCMD): (1) Feed; (2) permeate; (3) heating thermostat; (4) cooling thermostat; (5) double head peristaltic pump; (6) hollow fiber membrane module; (7) Pt-100 probes; (8) flow meter; (9) glass heat exchangers; (10) precision balance; (11) computer.

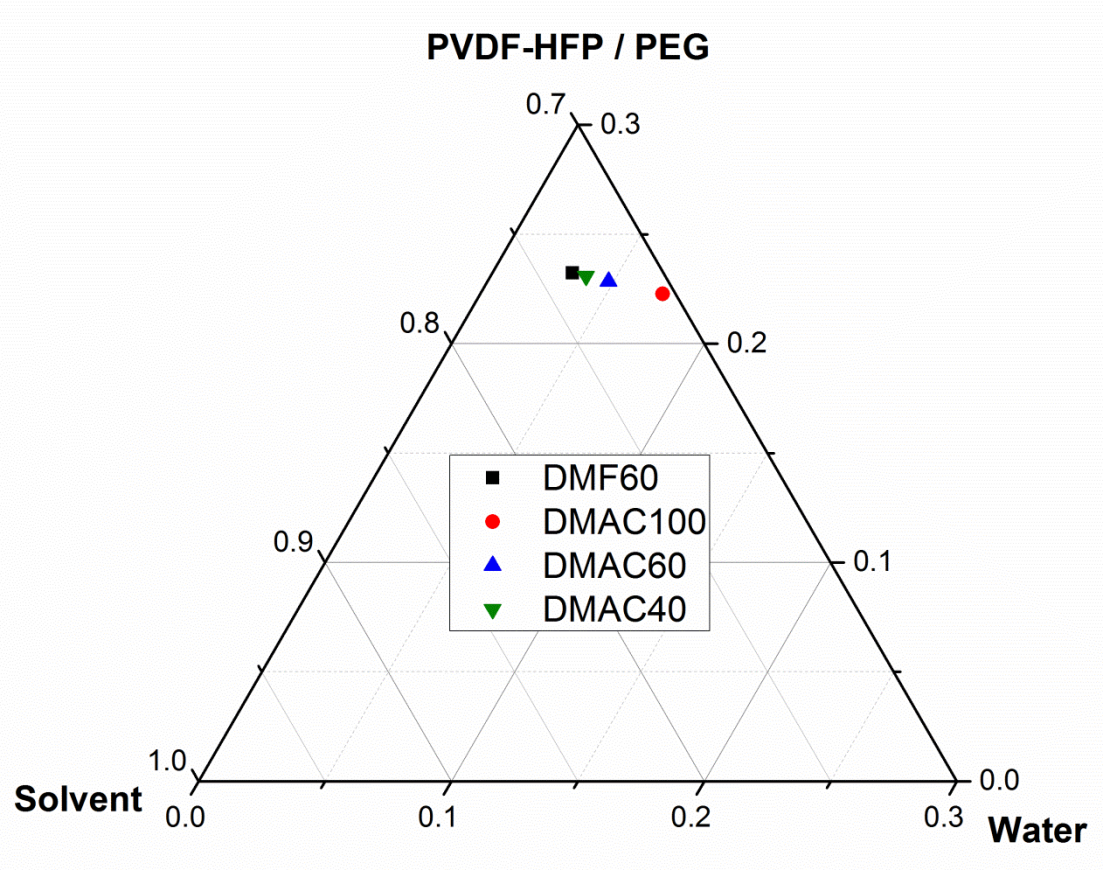

Figure 3. Ternary phase diagram of the (PVDF-HFP/PEG)/solvent (single and mixed solvents)/water systems.

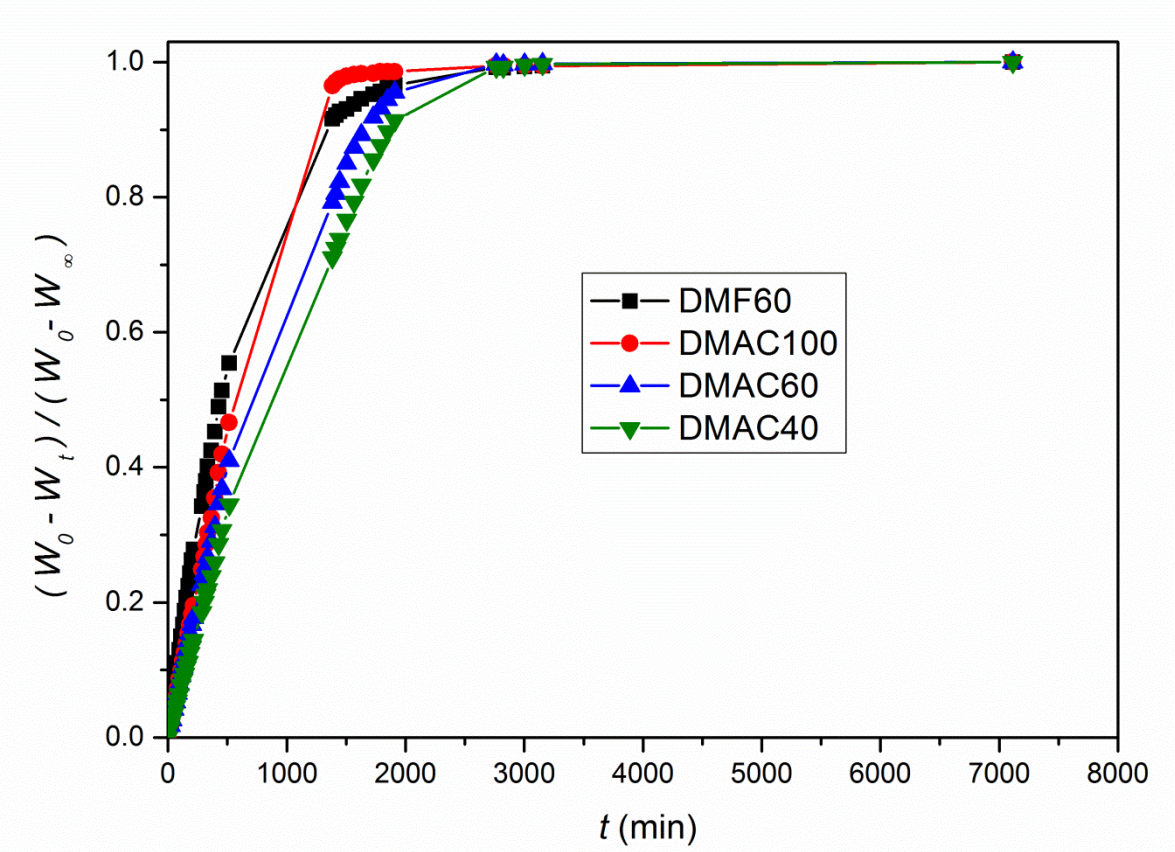

Figure 4. Experimental data of the weights variation $\left(\frac{W_0-W_t}{W_0-W_\infty}\right)$ of different spinning solutions with solvent(s) evaporation time.

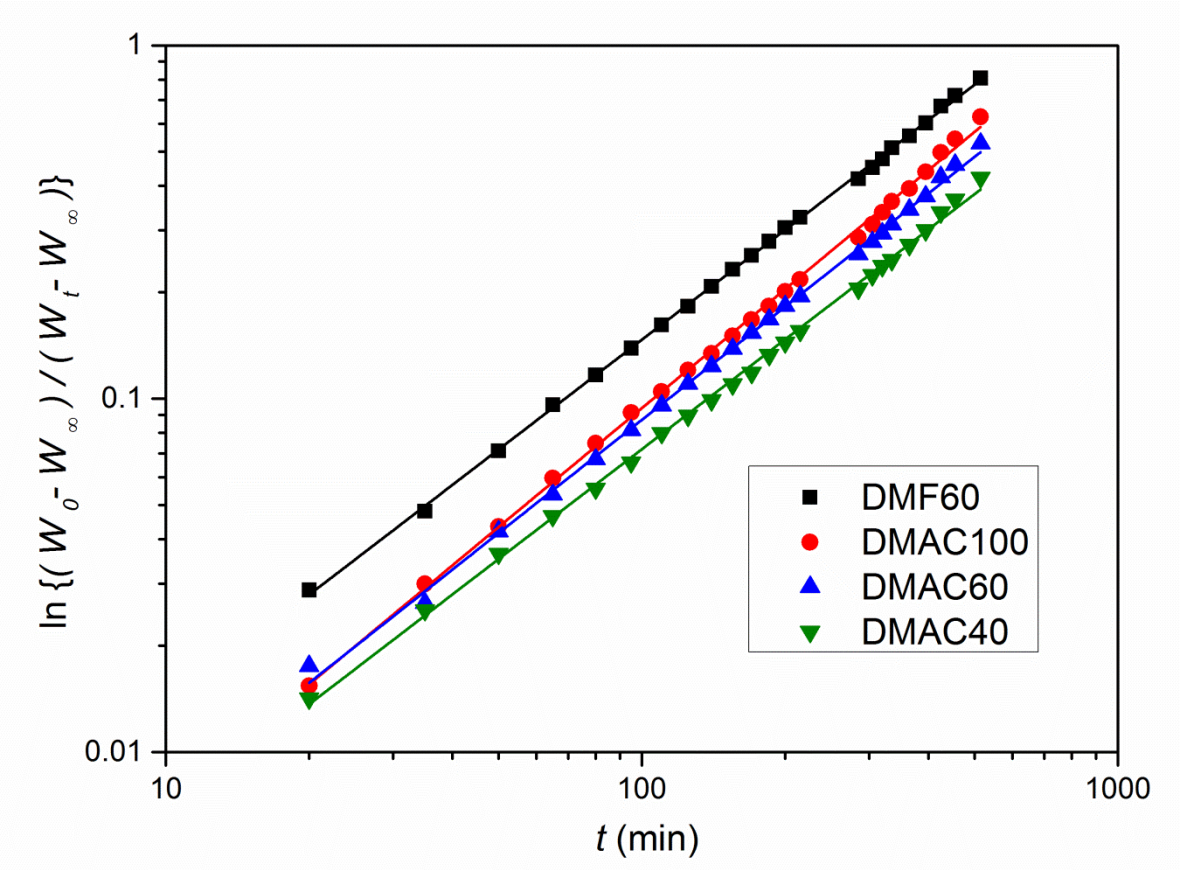

Figure 5. Logarithmic plot of $ln\left(\frac{W_0-W_\infty}{W_t-W_\infty}\right)$ *versus* time for the data shown in Fig. 4.

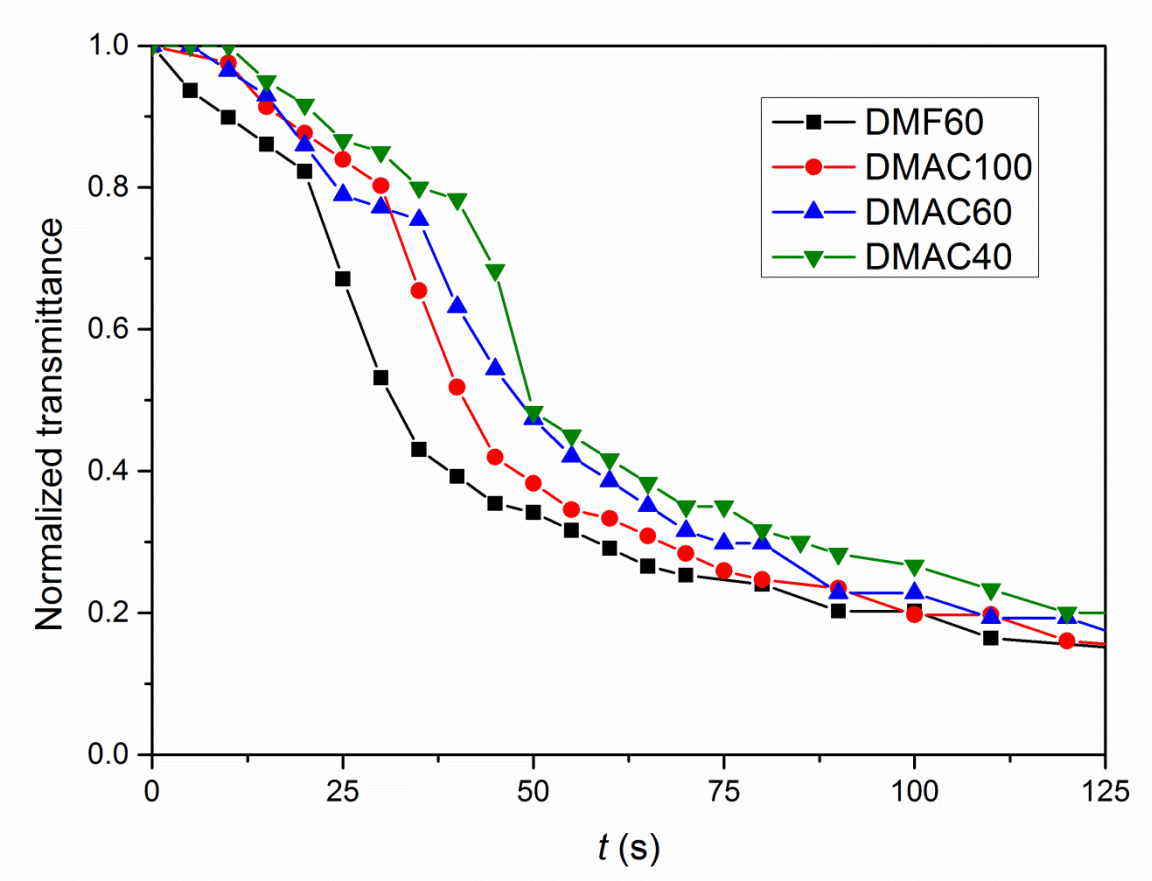

Figure 6. Coagulation experiments of the spinning solutions prepared with different solvents.

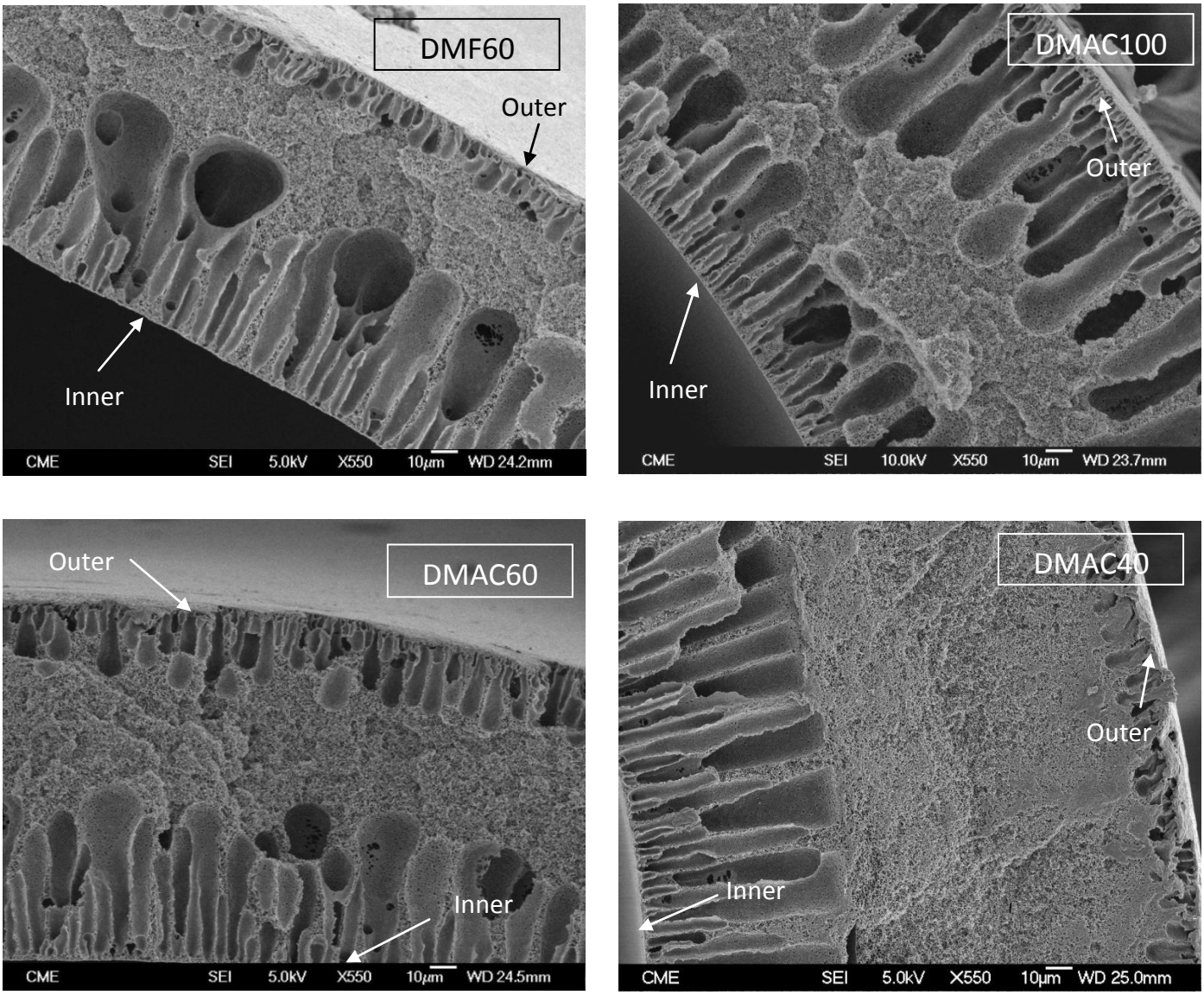

Figure 7. SEM images of the cross-section morphology of the PVDF-HFP hollow fiber membranes prepared with different solvents.

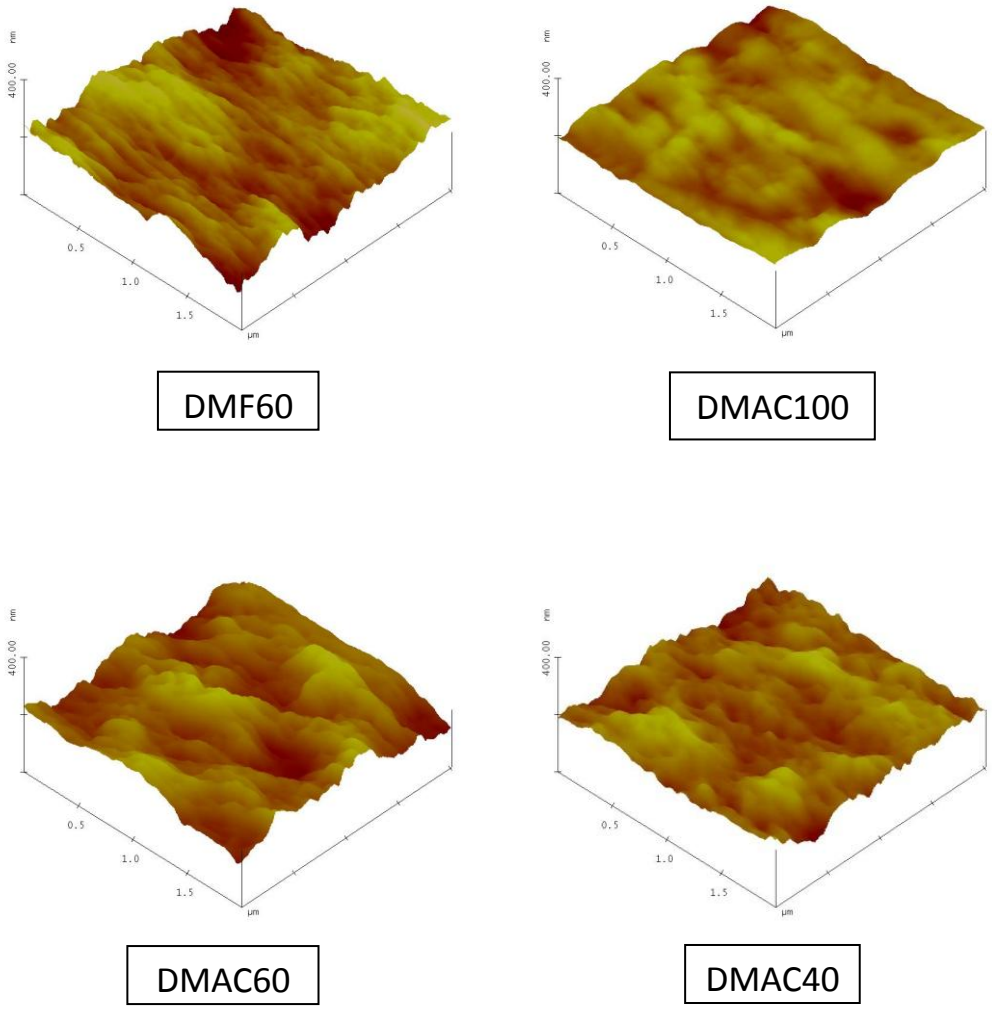

Figure 8. 3D AFM images of the inner surfaces of the PVDF-HFP hollow fiber membranes prepared with different solvents.

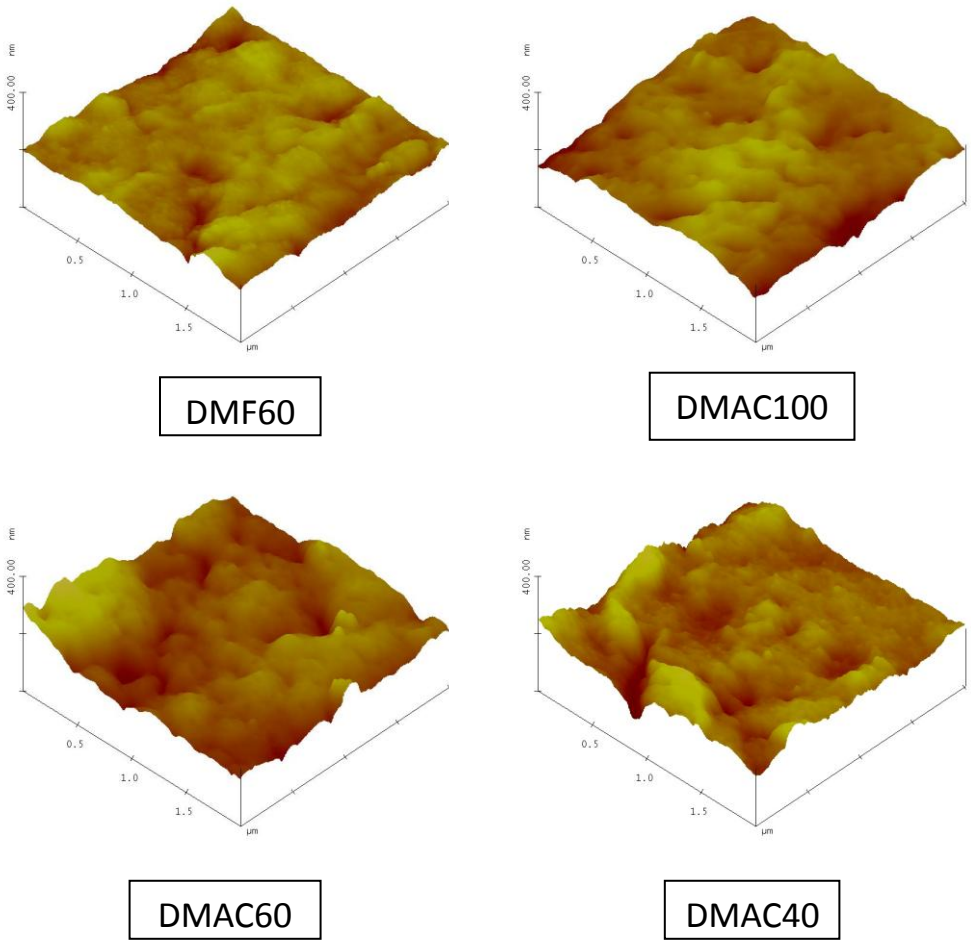

Figure 9. 3D AFM images of the outer surfaces of the PVDF-HFP hollow fiber membranes prepared with different solvents.

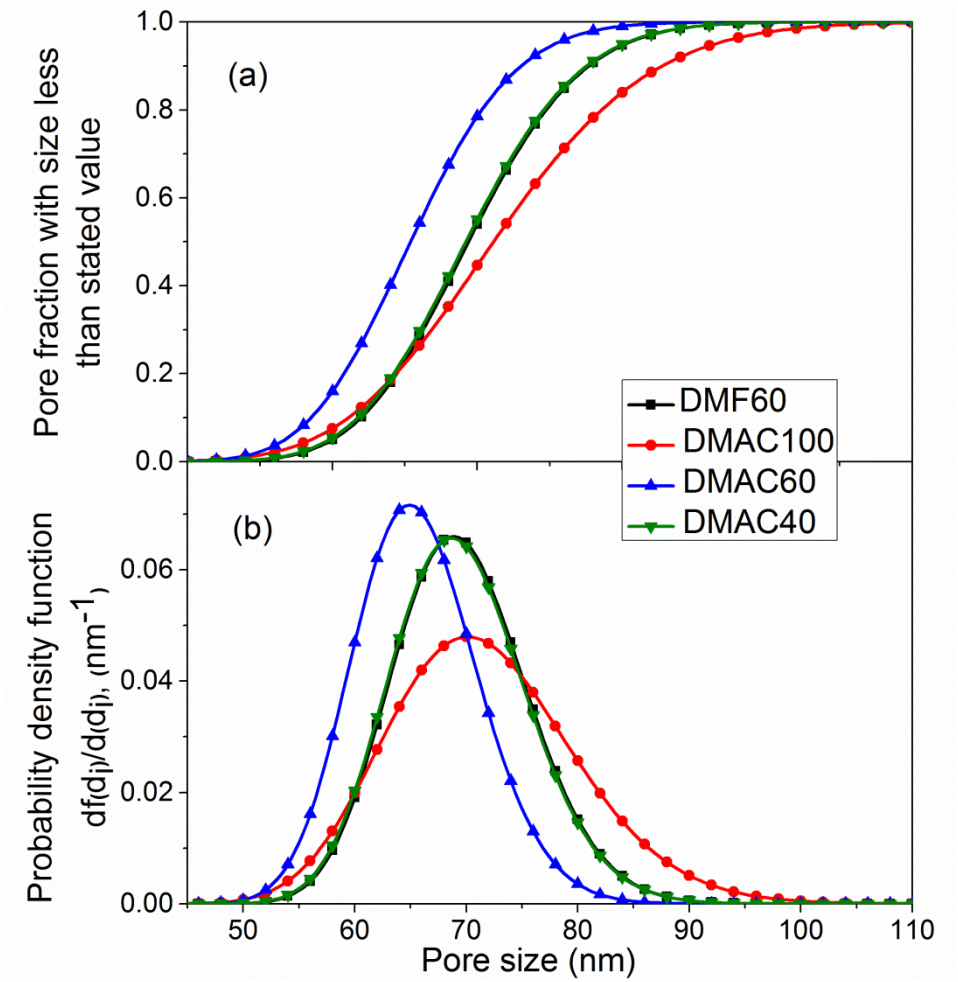

Figure 10. Cumulative pore size (a) and probability density function (b) curves generated from the pore sizes obtained from AFM images of the inner surfaces of the PVDF-HFP hollow fiber membranes prepared with different solvents.

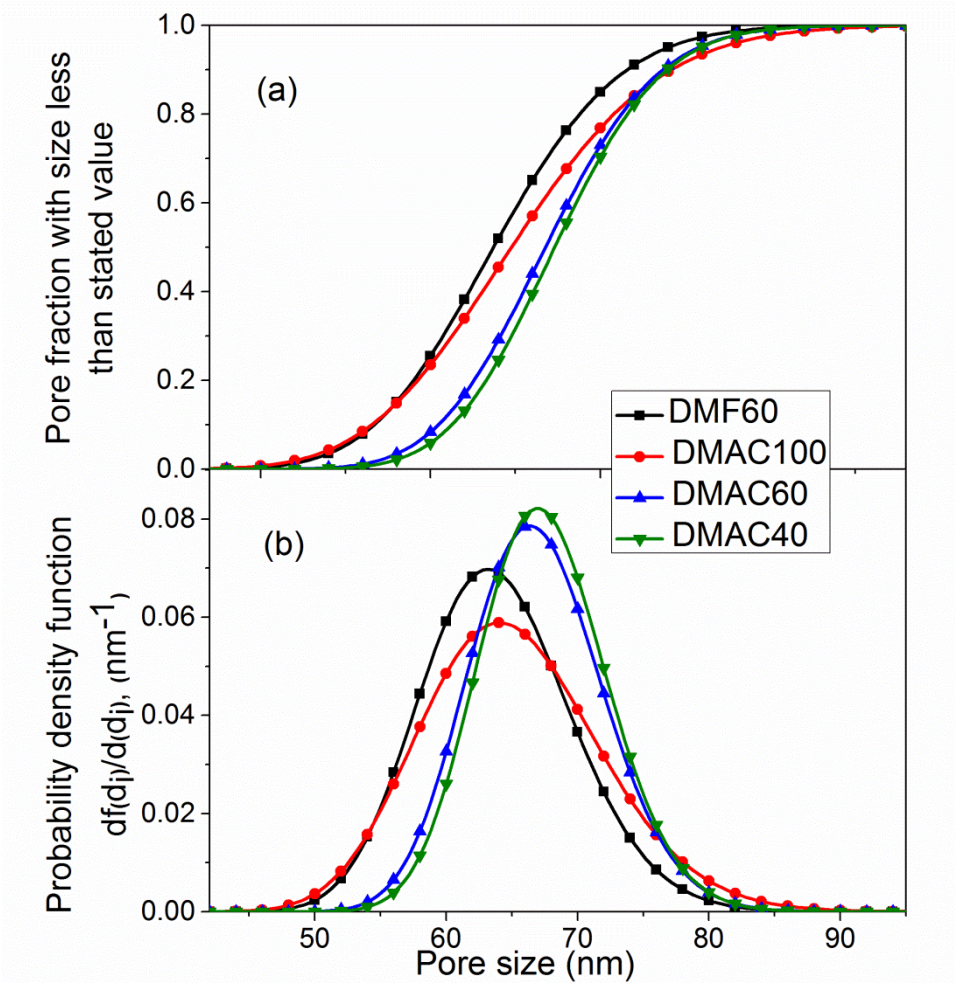

Figure 11. Cumulative pore size (a) and probability density function (b) curves generated from the pore sizes obtained from AFM images of the outer surfaces of the PVDF-HFP hollow fiber membranes prepared with different solvents.

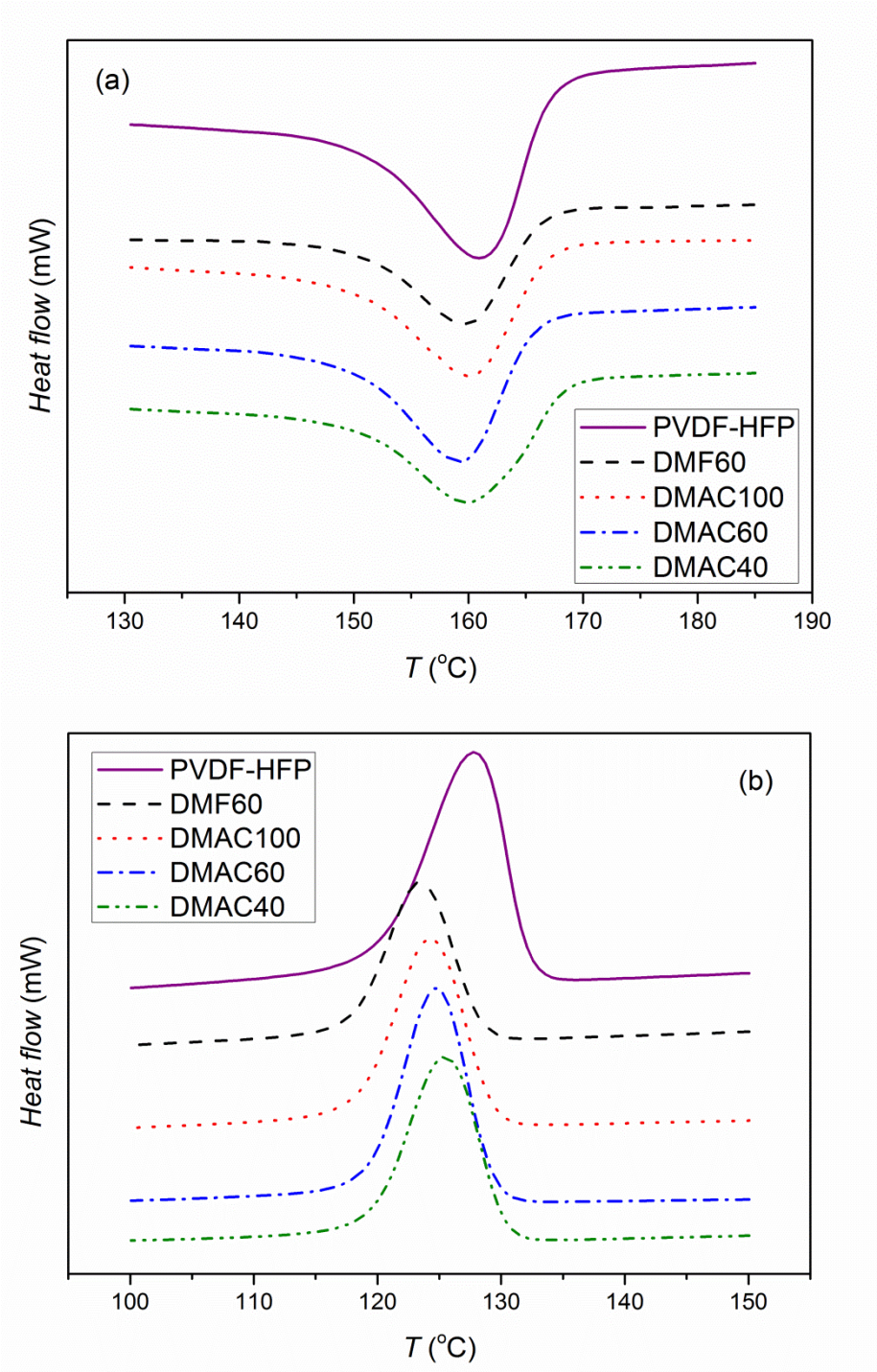

Figure 12. DSC thermograms, (a) heating and (b) cooling of the copolymer PVDF-HFP and the PVDF-HFP hollow fiber membranes prepared with different solvents.

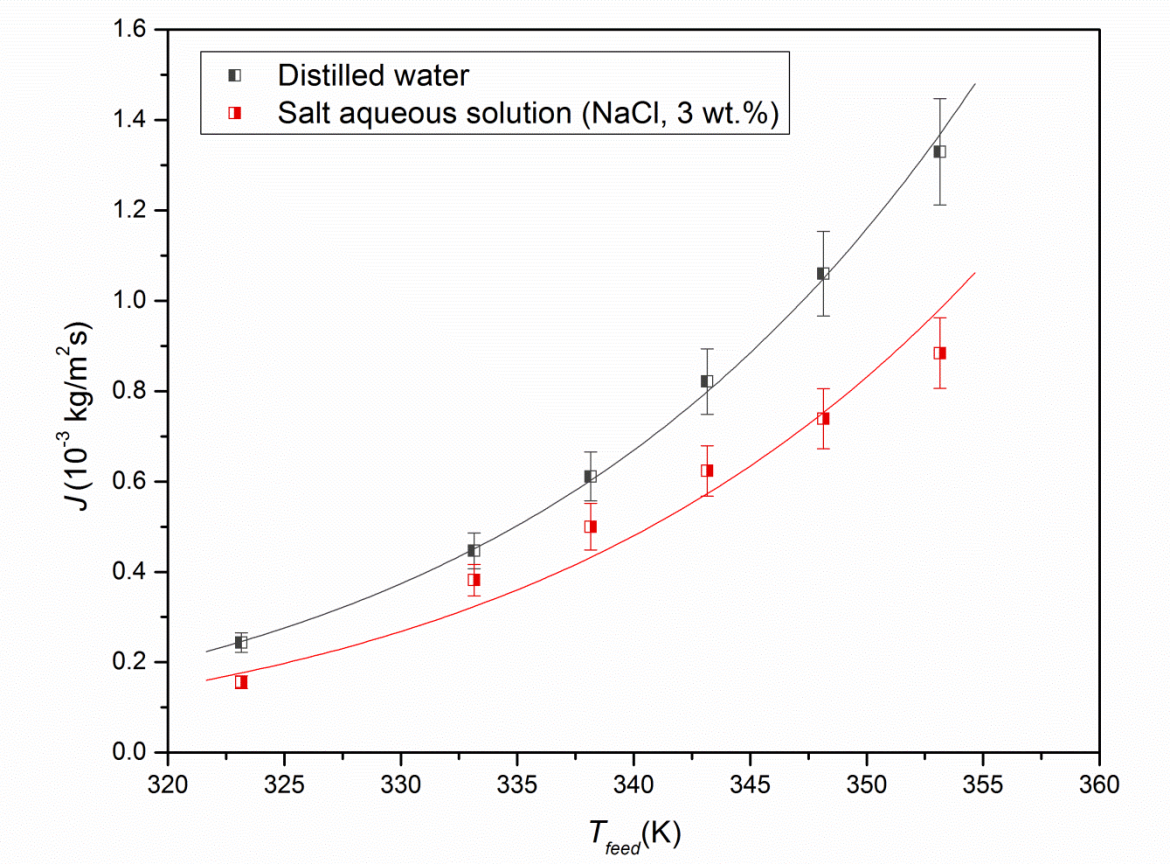

Figure 13. Effect of the feed inlet temperature on the DCMD permeate flux of the membrane DMF60. The permeate temperature was kept at 25 ^{o}C.

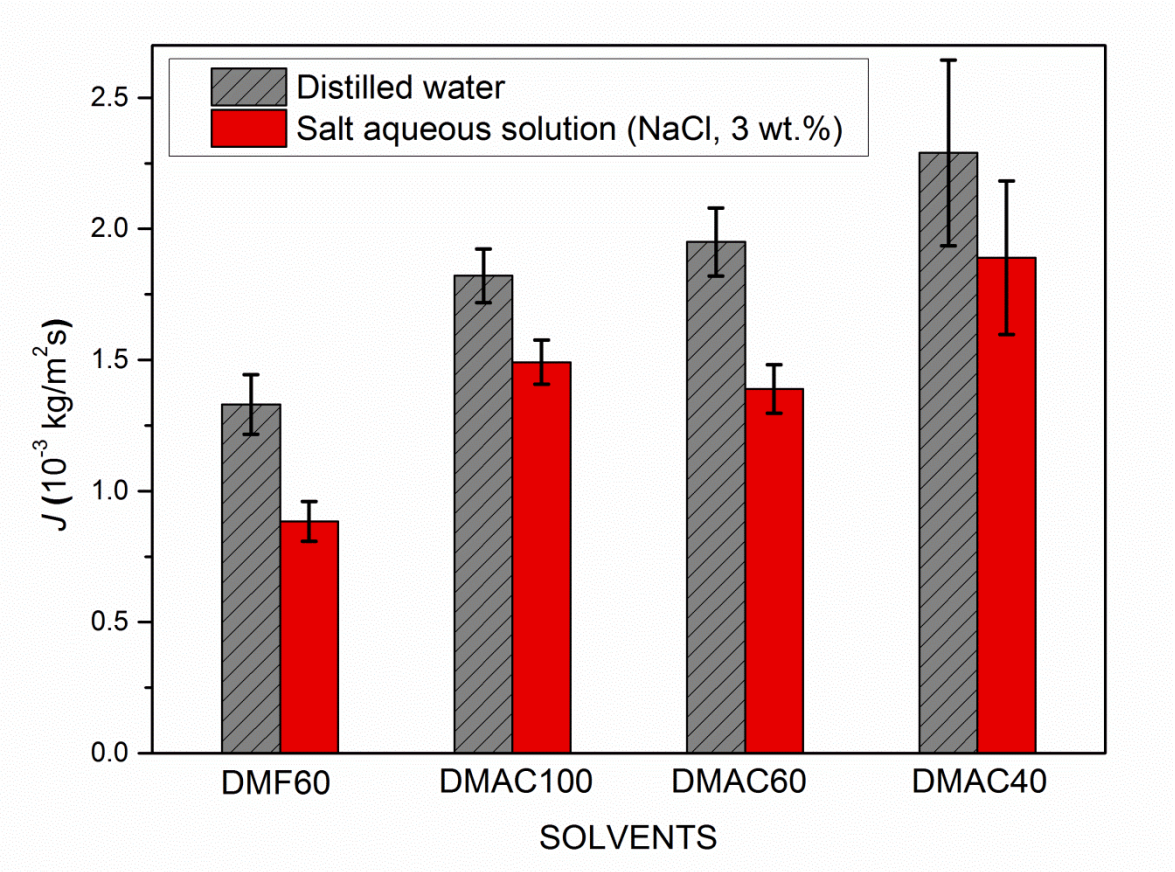

Figure 14. DMCD permeate flux of the PVDF-HFP hollow fiber membranes prepared with different solvents. (Feed temperature = 80^{o}C; Permeate temperature = 25^{o}C).

TABLES

Table 1. Composition of the spinning solutions, PVDF-HFP (19 wt.%) / PEG (5 wt.%) / Solvent (76 wt.%), their viscosity and surface tension.

Dope solutions	Solvents			Viscosity (mPa s)	Surface tension (mN/m)
	DMF (%)	DMAC (%)	TMP (%)		
DMF60	60		40	3956 ± 51	33.72 ± 0.17
DMAC100		100		3030 ± 79	33.68 ± 0.14
DMAC60		60	40	4942 ± 66	31.74 ± 0.07
DMAC40		40	60	5792 ± 62	30.45 ± 0.20

Table 2. Spinning parameters of PVDF-HFP hollow fiber membranes.

Parameters	Operating conditions
Inner and outer diameter of the spinneret	d_i = 1.0 mm / d_e = 2.4 mm
Extrusion pressure (kPa)	60
Polymeric solution flow rate (m^3/s)	$2.8\ 10^{-8}$
Polymeric solution temperature (ºC)	42
Bore fluid	Distilled water
Bore fluid flow rate (m^3/s)	$3.2\ 10^{-7}$
External coagulant	Tap water
Bore fluid and external coagulation temperature (ºC)	42
Air gap distance (m)	0.275
Take-up speed (m/s)	0.16
Post-treatment	Tap water

Table 3. Solubility parameters of the solvents, the solvents mixture, the additive PEG, the nonsolvent water and PVDF-HFP with their HSP distances (R_{HSP}) and diffusion coefficients of the solvents.

Material	Solubility parameters ($MPa^{1/2}$)			R_{HSP} [a] ($MPa^{1/2}$)		Diffusion coefficients (10^6 cm^2/s) [52]
	δ_D	δ_P	δ_H	*P-S* [c]	*W- S* [d]	D_m
DMF [47]	17.4	13.7	11.3	9.8	31.3	12.8
DMAC [47]	16.8	11.5	10.2	7.2	32.5	11.8
TMP [47]	16.7	15.9	10.2	10.4	32.2	8.6
Water [47]	15.5	16	42.3	---	---	
PEG [31]	15.3	9.6	8.5	---	---	
PVDF-HFP [49]	15.3	7.2	5.3	---	---	
DMF60[b]	17.2	14.5	10.9	9.9	31.6	
DMAC100 [b]	16.8	11.5	10.2	7.2	32.5	
DMAC60 [b]	16.8	13.0	10.2	8.1	32.3	
DMAC40 [b]	16.7	13.9	10.2	8.8	32.3	

[a] Calculated using Eq. (3).
[b] Calculated using Eq. (4).
[c] *P-S*: PVDF-HFP-solvent interaction.
[d] *W-S*: water-solvent interaction.

Table 4. Empirical parameters (*m* and *b* in Eq. (5)) of the PVDF-HFP spinning solutions.

Spinning solution	*m*	*b* (10^{-4} min^{-m})
DMF60	1.0377 ± 0.0050	12.229 ± 0.048
DMAC100	1.1163 ± 0.0096	5.515 ± 0.037
DMAC60	1.0847 ± 0.0071	5.798 ± 0.029
DMAC40	1.0395 ± 0.0099	5.965 ± 0.042

Table 5. Diameters, thickness, void volume fraction and *LEP* of PVDF-HFP hollow fibers membranes.

Membrane	Inner diameter (μm)	Outer diameter (μm)	Thickness (μm)	Void volume fraction (ε %)	*LEP* (10^5 Pa)
DMF60	1515 ±130	1800 ± 100	141 ± 19	67.3 ± 2.4	0.95 ± 0.06
DMAC100	1310 ± 70	1610 ± 80	150 ± 50	72.5 ± 1.1	2.04 ± 0.04
DMAC60	1470 ± 100	1700 ± 130	113 ± 16	65.1 ± 2.2	1.00 ± 0.05
DMAC40	1190 ± 180	1550 ± 150	180 ± 40	70.9 ± 1.2	1.04 ± 0.04

Table 6. Minimum, maximum and average mean roughness parameter, R_a, together with the corresponding standard deviation of the internal and external surfaces of the PVDF-HFP hollow fibers prepared with different solvents (scan range considered 2μm × 2μm).

Membrane	R_a (nm) Inner surface			R_a (nm) Outer surface		
	Minimum	Maximum	Average	Minimum	Maximum	Average
DMF60	10.0	22.2	15.7 ± 4.1	8.1	22.4	15.7 ± 5.0
DMAC100	10.2	15.4	12.6 ± 1.9	12.6	23.5	17.1 ± 3.0
DMAC60	11.6	28.0	20.2 ± 4.4	16.9	25.9	21.6 ± 3.3
DMAC40	13.9	18.6	15.8 ± 2.0	15.8	29.9	22.5 ± 4.3

Table 7. Mean pore size, μ_p, and geometric standard deviation, σ_p, of the internal and external surfaces of the PVDF-HFP hollow fiber membranes determined by AFM images analysis.

Membrane	Inner surface		Outer surface	
	μ_p(nm)	σ_p(nm)	μ_p(nm)	σ_p(nm)
DMF60	69.38	1.09	63.71	1.09
DMAC100	71.11	1.12	64.76	1.11
DMAC60	65.38	1.09	66.76	1.08
DMAC40	69.20	1.09	67.31	1.07

Table 8. Mean pore radius, r_p, and effective porosity, ε/L_p, of the PVDF-HFP hollow fiber membranes determined from wet and dry curves obtained by Porometry test.

Membrane	Wet curve	Dry curve	
	r_p (nm)	r_p (nm)	ε/L_p (m^{-1})
DMAC100	114.8 ± 1.1	121 ± 6	277 ± 29
DMAC60	141.8 ± 1.1	141 ± 4	276 ± 19
DMAC40	188.7 ± 1.1	177 ± 3	193± 7

Table 9. Melting temperature (T_m), crystallization temperature (T_c), enthalpy of melting (ΔH_m), enthalpy of crystallization (ΔH_m) and crystallinity (X_c) of the PVDF-HFP copolymer and the hollow fiber membranes prepared with different solvents.

Sample	Heating process		Cooling process		Crystallinity
	$\Delta H_m \pm 0{,}5$ (J/g)	$T_m \pm 0{,}15$ (^{o}C)	$\Delta H_c \pm 0{,}5$ (J/g)	$T_c \pm 0{,}15$ (^{o}C)	X_c (%) [a]
PVDF-HFP	29.0	161.41	29.4	128.00	27.68
DMF60	28.0	159.53	23.7	123.85	26.76
DMAC100	29.7	160.18	29.8	124.17	28.36
DMAC60	29.9	159.42	31.1	124.94	28.52
DMAC40	32.7	159.69	32.2	125.43	31.23

[a] Calculated using Eq. (2).